

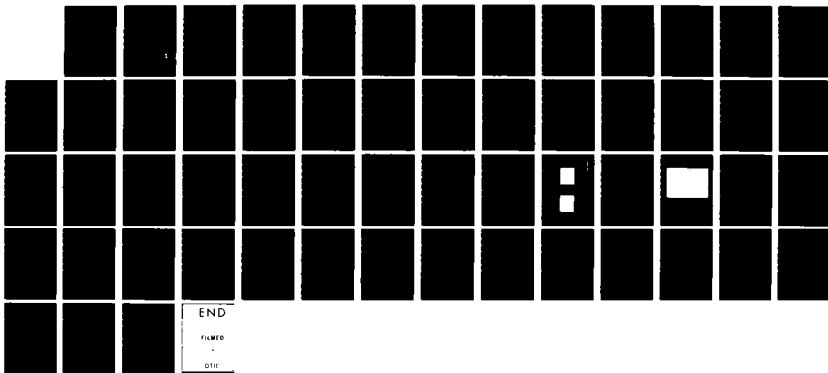
AD-A124 193

EFFICIENT RAMAN CONVERSION OF XEC1 LASER INTO THE
BLUE-GREEN REGION(U) NORTHROP RESEARCH AND TECHNOLOGY
CENTER PALOS VERDES PENINSUL... H KOMINE ET AL NOV 82
NRTC-82-24R N00014-81-C-0293 F/G 28/5

1/1

UNCLASSIFIED

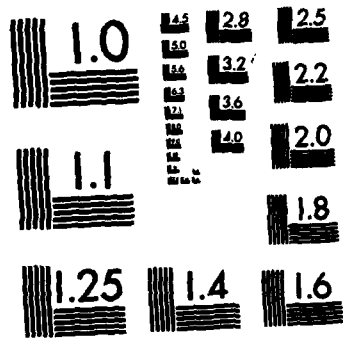
NL



END

FILMED

DTIC



MICROCOPY RESOLUTION TEST CHART
NATIONAL BUREAU OF STANDARDS-1963-A

12

NRTC-82-24R

ADA 124193

EFFICIENT RAMAN CONVERSION OF XeCl LASER
INTO THE BLUE-GREEN REGION

November 1982

Prepared by

Laser Technology Laboratory
Northrop Corporation
Northrop Research and Technology Center
One Research Park
Palos Verdes Peninsula, California 90274

DTIC
ELECTRONIC
S FEB 7 1983
A

DTIC FILE COPY

This document has been approved
for public release and sale; its
distribution is unlimited.

83 02 07 023

REPORT DOCUMENTATION PAGE		READ INSTRUCTIONS BEFORE COMPLETING FORM
1. REPORT NUMBER NRTC-82-24R	2. GOVT ACCESSION NO. AD-A124193	3. RECIPIENT'S CATALOG NUMBER
4. TITLE (and Subtitle) Efficient Raman Conversion of XeCl Laser Into the Blue-Green Region		5. TYPE OF REPORT & PERIOD COVERED Final
		6. PERFORMING ORG. REPORT NUMBER
7. AUTHOR(s) Hiroshi Komine and Eddy A. Stappaerts		8. CONTRACT OR GRANT NUMBER(s) N00014-81-C-0293
9. PERFORMING ORGANIZATION NAME AND ADDRESS Northrop Research and Technology Center One Research Park Palos Verdes Peninsula, CA 90274		10. PROGRAM ELEMENT, PROJECT, TASK AREA & WORK UNIT NUMBERS
11. CONTROLLING OFFICE NAME AND ADDRESS Office of Naval Research 800 North Quincy Street Arlington, VA 22217		12. REPORT DATE
		13. NUMBER OF PAGES 50
14. MONITORING AGENCY NAME & ADDRESS (if different from Controlling Office) Naval Ocean Systems Center 271 Catalina Boulevard San Diego, CA		15. SECURITY CLASS. (of this report) UNCLASSIFIED
		15a. DECLASSIFICATION/DOWNGRADING SCHEDULE
16. DISTRIBUTION STATEMENT (of this Report) Distribution Unlimited		
17. DISTRIBUTION STATEMENT (of the abstract entered in Block 20, if different from Report)		
18. SUPPLEMENTARY NOTES		
19. KEY WORDS (Continue on reverse side if necessary and identify by block number) Blue-Green Laser; UV Excimer Laser; Raman Shifting		
20. ABSTRACT (Continue on reverse side if necessary and identify by block number) An efficient, blue-green laser source is urgently needed for the Navy submarine communication system as well as other applications. The rare-gas halide excimer lasers developed over the last few years appear to meet the requirements on efficiency and scalability, but the wavelength of their near-uv emission is too short for direct use. This report describes theoretical and experimental work on the feasibility of a novel, frequency conversion scheme, based on higher order Raman scattering, for		

efficiently shifting the uv wavelengths of these excimer lasers to the blue-green region.

The technique uses an oscillator-amplifier combination, and the Raman medium is typically a gas such as hydrogen or deuterium at a pressure of several atmospheres. In preliminary experiments with a frequency-tripled Nd:YAG laser (355 nm), photon efficiencies as high as 51 percent have been obtained for the second Stokes order, in very good agreement with computer simulations.

More recently, the Raman oscillator-amplifier experiments have been extended to the case of an XeCl pump laser. The Raman amplifier experiments led to the observation of significant conversion from 308 nm to 499 nm by third Stokes order shifting for the first time. Energy conversion measurements have yielded up to 14 percent amplifier efficiency which was limited by the available pump energy and focusing geometry and the short pulses in the present experiment. For longer, rectangular pulses the energy conversion is expected to nearly equal the peak power efficiencies. Furthermore, the use of a collimated uniform beam profile for the pump laser, as obtained with large Fresnel number unstable resonators, is also predicted to improve the conversion efficiency up to values approaching the quantum limit.

The use of an oscillator-amplifier combination, as compared to an oscillator, results in higher efficiency, greatly reduced beam divergence, and typically an order of magnitude reduction of the energy loading on the Raman converter windows. This approach is applicable to various Raman media including molecular gases, liquids, and metal vapors. In the case of molecular gases, four-wave mixing processes can distribute the energy between several Stokes orders in Raman oscillators employing vibrational scattering. However, this effect is reduced to negligible values in the oscillator-amplifier scheme because of the much lower pump intensities in the amplifier. The use of collimated beams further decreases the role of these processes.

During the experimental investigation of the oscillator-amplifier scheme, the pump laser bandwidth was found to have a major effect on the amplifier gain. A comprehensive analytical model has been developed which explains these observations in terms of the interference between the various longitudinal modes of the pump and Stokes waves.

The analysis of the effects of broadband pump laser has also included nonlinear dispersion in the Raman medium. This dispersion arises from the real part of the Raman susceptibility tensor, and its magnitude depends on the pump intensity. Thus, spatially non-uniform pump beams can cause varying phase shifts across an amplified Stokes wavefront, which lead to beam quality degradation. However, detailed computer code calculations indicated that these phase shifts may be small in an amplifier with strong pump depletion. This suggested that high efficiency Stokes conversion is feasible with good beam quality output.

Based on the experimental results and theoretical analyses, a Joule-level blue-green Raman converter point design is presented for an XeCl pump laser. For moderate and high average power operations, it is recommended that a suitable Raman cell with flowing H₂ gas be used to maintain conversion efficiency and beam quality.

NRTC-82-24R

EFFICIENT RAMAN CONVERSION OF XeCl LASER
INTO THE BLUE-GREEN REGION

November 1982

Prepared by

Laser Technology Laboratory
Northrop Corporation
Northrop Research and Technology Center
One Research Park
Palos Verdes Peninsula, California 90274



Accession For	
NTIS GRA&I	<input checked="" type="checkbox"/>
DTIC TAB	<input type="checkbox"/>
Unannounced	<input type="checkbox"/>
Justification	
By	
Distribution/	
Availability Codes	
Dist	Avail and/or Special
A	

TABLE OF CONTENTS

LIST OF FIGURES	11
1.0 SUMMARY	1
2.0 BACKGROUND	4
3.0 THEORETICAL ANALYSES AND EXPERIMENTS	7
3.1 Experiments with Nd:YAG/Third Harmonic Pump.	7
3.2 Raman Amplifier Analysis	13
3.2.1 Broadband Raman Scattering	14
3.2.2 Gain Enhancement by Temporal Matching	18
3.2.3 Multiple Stokes Raman Amp. Computer Sim.	22
3.3 XeCl Laser Raman Conversion	25
3.3.1 Narrow Bandwidth XeCl Laser System	26
3.3.2 Raman Oscillator-Amplifier System	28
3.4 Nonlinear Dispersion in Broadband Amplifiers	36
3.4.1 Coupled-Mode Analysis	37
3.4.2 Broadband Multiple-Stokes Amplification	40
4.0 BLUE-GREEN RAMAN CONVERTER DESIGN	43
5.0 CONCLUSIONS	49
6.0 REFERENCES	50

LIST OF FIGURES

Figure		Page
1	Schematic of Excimer Laser and Frequency Converter	5
2	Third-Order Raman Amplifier Photon Efficiency vs Amplifier Length	6
3	Multiple Stokes Raman Oscillator-Amplifier Experimental Layout	8
4	Oscillator Energy Conversion Efficiency vs Pump Energy	9
5	Amplifier Energy Conversion vs Pump Energy	10
6	Amplified Stokes Pulses and Pump Depletion	11
7	Amplifier Energy Conversion vs Pump Energy	12
8	Raman Amplifier Analysis	13
9	Laser-Bandwidth Dependence of Forward Gain in a Raman Amplifier with Uncorrelated Injected Phases	17
10	Schematic of the Temporal Matching Experiment	19
11	Amplified Stokes Energy vs Optical Delay For Pump Bandwidth (a) 0.33 cm^{-1} (b) 0.86 cm^{-1}	19
12	Raman Amplifier Gain vs Pump Energy	21
13	H ₂ Raman Amplifier Power Conversion vs Gain for Uniform Beam Profile	24
14	H ₂ Raman Amplifier Power Conversion vs Gain for Uniform Beam Profile	24
15	Raman Amplifier Energy Conversion vs Gain in H ₂ : Gaussian Pulse Simulation	25
16	Raman Conversion of XeCl Laser Experimental Configuration	27
17	Pulsed Dye Oscillator-Amplifier System With SHG	27
18	XeCl Laser/Amplifier Spectrum	29

LIST OF FIGURES (CONT'D.)

Figure		Page
19	Raman Converter Configuration	30
20	Photograph of Raman Oscillator-Amplifier Setup	31
21	H ₂ Raman Amplifier Energy Conversion vs Pump Energy	33
22	Pump Input and Amplified Third Stokes Pulses	34
23	H ₂ Raman Amplifier Power Conversion vs Gain for Gaussian Beam Profile	35
24	Re $\chi^{(3)}$ and Im $\chi^{(3)}$ of H ₂ Q ₀₁ (1) Transition	36
25	RMS Intensity-Averaged Phase Increment in Small-Signal Regime	38
26	RMS Phase in Saturated Regime	39
27	Stokes Amplification Dependence on Pump Spectrum Bandwidth	40
28	XeCl Third-Stokes Conversion in Hydrogen	41
29	XeCl Third Stokes Conversion in Hydrogen	42
30	XeCl Pump Laser Characteristics for a Joule-Level Blue-Green Converter	43
31	Third Stokes Power Conversion Efficiency vs Normalized Injection Level	44
32	Pulse Shape and Energy Efficiency Simulation for a Peak Gain of G = 29	45
33	Pulse Shape and Energy Efficiency Simulation for a Peak Gain of G = 35	46
34	Blue-Green Raman Converter Point Design Parameters	46
35	Blue-Green Raman Converter Point Design Schematic	47
36	Blue-Green Raman Converter Point Design Optical Train Phase Error Budget	47

1.0 SUMMARY

An efficient, blue-green laser source is urgently needed for the Navy submarine communication system as well as other applications. The rare-gas halide excimer lasers developed over the last few years appear to meet the requirements on efficiency and scalability, but the wavelength of their near-uv emission is too short for direct use. This report describes theoretical and experimental work performed at Northrop Research and Technology Center (NRTC) on the feasibility of a novel frequency conversion scheme, based on higher order Raman scattering, for efficiently shifting the uv wavelengths of these excimer lasers to the blue-green region.

The technique uses an oscillator-amplifier combination, and the Raman medium is typically a gas such as hydrogen or deuterium at a pressure of several atmospheres. In preliminary experiments [KS79] with a frequency-tripled Nd:YAG laser (355 nm), photon efficiencies as high as 51 percent have been obtained for the second Stokes order, in very good agreement with computer simulations. The laser pulse length in these initial experiments was very short (6 ns), which limits the amplifier efficiency because of reduced Raman gain at the leading and trailing edges of the pulse.

More recently the Raman oscillator-amplifier experiments have been extended to the case of an XeCl pump laser [KS82]. In these experiments the pump radiation at 308 nm has been spectrally narrowed to about 0.4 cm^{-1} (0.04 \AA) by operating the XeCl laser as an amplifier whose input radiation is obtained from a frequency doubled narrow bandwidth dye laser system. Although short pulse lengths ($\sim 8 \text{ ns}$) have been used, the Raman oscillator showed efficient operation with outputs of up to fourth Stokes order in H_2 gas. Similarly, the Raman amplifier experiments led to the observation of significant conversion from 308 nm to 499 nm by third Stokes order shifting for the first time. Energy conversion measurements have yielded up to 14 percent amplifier efficiency

which was limited by the available pump energy and focusing geometry and the short pulses in the present experiment. In particular, the buildup time of Raman conversion into the third Stokes has been observed to be about 2 to 3 nanoseconds, which caused the 499 nm radiation to exhibit 5 to 6 nanosecond duration. This indicated that peak power conversion of about 25 percent has been demonstrated in reasonable agreement with a model calculation for the present case. For longer, rectangular pulses the energy conversion is expected to nearly equal the peak power efficiencies. Furthermore, the use of a collimated uniform beam profile for the pump laser, as obtained with large Fresnel number unstable resonators, is also predicted to improve the conversion efficiency up to values approaching the quantum limit.

The use of an oscillator-amplifier combination, as compared to an oscillator, results in higher efficiency, greatly reduced beam divergence, and typically an order to magnitude reduction of the energy loading on the Raman converter windows. This approach is applicable to various Raman media including molecular gases, liquids, and metal vapors. In the case of molecular gases, four-wave mixing processes can distribute the energy between several Stokes orders in Raman oscillators employing vibrational scattering. However, this effect is reduced to negligible values in the oscillator-amplifier scheme because of the much lower pump intensities in the amplifier. The use of collimated beams further decreases the role of these processes.

During the experimental investigation of the oscillator-amplifier scheme, the pump laser bandwidth was found to have a major effect on the amplifier gain. A comprehensive analytical model has been developed which explains these observations in terms of the interference between the various longitudinal modes of the pump and Stokes waves. In addition, a gain enhancement technique [SLK80] which increases broadband gains to the value observed for monochromatic pumping, was predicted and demonstrated. This technique has also been utilized in the recent experiments with

the XeCl laser. Although the new technique can eliminate the need for narrow bandwidth, injection-locking will probably be necessary for the Navy application with respect to maximizing the signal-to-noise ratio of the receiver.

The analysis of the effects of broadband pump laser has also included nonlinear dispersion in the Raman medium. This dispersion arises from the real part of the Raman susceptibility tensor, and its magnitude depends on the pump intensity. Thus, spatially non-uniform pump beams can cause varying phase shifts across an amplified Stokes wavefront, which lead to beam quality degradation. However, detailed computer code calculations indicated that these phase shifts may be small in an amplifier with strong pump depletion. This suggested that high efficiency Stokes conversion is feasible with good beam quality output.

Based on the experimental results and theoretical analyses, a Joule-level blue-green Raman converter point design is presented for an XeCl pump laser. For moderate and high average power operations, it is recommended that a suitable Raman cell with flowing H_2 gas be used to maintain conversion efficiency and beam quality.

2.0 BACKGROUND

The Raman oscillator-amplifier concept is generally applicable in various media [GZ78]. In atomic vapors, large electronic Raman shifts are adequate to convert uv wavelengths into the visible region in a single Stokes shift [BD79]. In contrast, Raman shifting in gases such as H_2 , D_2 , HD, etc. require multiple Stokes shifts to generate the visible output [LSB79]. A list of wavelengths which can be generated starting from an XeCl or XeF laser, using these Raman media, is shown in Table 1, together with the quantum-efficiency for each case.

TABLE 1. LIST OF RAMAN SHIFTED WAVELENGTHS (Å)
IN THE BLUE-GREEN REGION STARTING FROM
XeCl AND XeF

Combination	Order of Process	XeCl ₂ (3080 Å)	XeF ₂ (3510 Å)	Quantum Efficiency
2 H ₂	2		4955	71
H ₂ + HD			4827	73
2 HD			4706	75
H ₂ + D ₂			4685	75
HD + D ₂			4572	77
2 D ₂				4443
3 H ₂	3	4999		62
2 H ₂ + HD		4869		63
2 H ₂ + D ₂		4724		65
3 HD		4628		67

A schematic of the complete system is shown in Figure 1. It consists of an excimer laser (XeCl, XeF), two Raman cells, and optical components. A small fraction of the laser output is sent through a beam reducing telescope, T_1 , and focused into a single-pass Raman oscillator cell through lens L_1 . This oscillator is operated several times above threshold, such that its output consists of 3 to 4 Stokes orders, each with an energy on the order of 10 to 25 percent of the laser energy. Near-diffraction-limited beams can be obtained from this oscillator through the use of a tight focusing geometry. The Stokes beams are recollimated with lens L_2 , sent through a filter, F , which transmits all orders up to the selected one but stops all the higher ones, and injected in the amplifier cell, RA, through a beam combining mirror, BC.

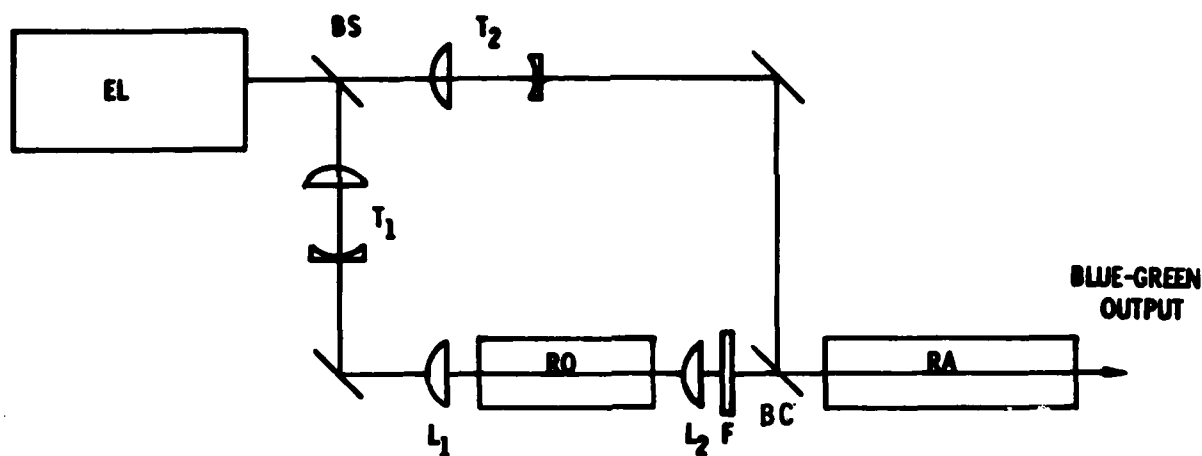


FIGURE 1. SCHEMATIC OF EXCIMER LASER AND FREQUENCY CONVERTER. EL - EXCIMER LASER, F - FILTER, BC - BEAM COMBINER, T_1/T_2 - TELESCOPES, L_1/L_2 - LENSES, RO - RAMAN OSCILLATOR, RA - RAMAN AMPLIFIER

As the pump beam and the injected Stokes beams travel through the amplifier, a sequential energy transfer takes place from one order to the next one, until most of the pump laser energy has been transferred to the selected order. A typical example of photon conversion is shown in Figure 2, which applies to the case

of a third-order shifter. It should be noted that, even though no energy is injected at orders higher than the third one, radiation at such wavelengths can still be generated through four-wave mixing processes. As is illustrated in Figure 2, if the amplifier gain is sufficiently high, this unwanted radiation can be further amplified by stimulated Raman scattering, thus resulting in a lower efficiency for the selected third order. For this reason, the gain must be kept within a certain range, typically within $\pm 40\%$ of the mean value. In practice, this requires the use of nearly rectangular beam and pulse profiles, and shot-to-shot power fluctuations within the above range. The efficiency of the undesired mixing processes can further be minimized through the use of nearly collimated beams in the amplifier since this eliminates angular phase-matching.

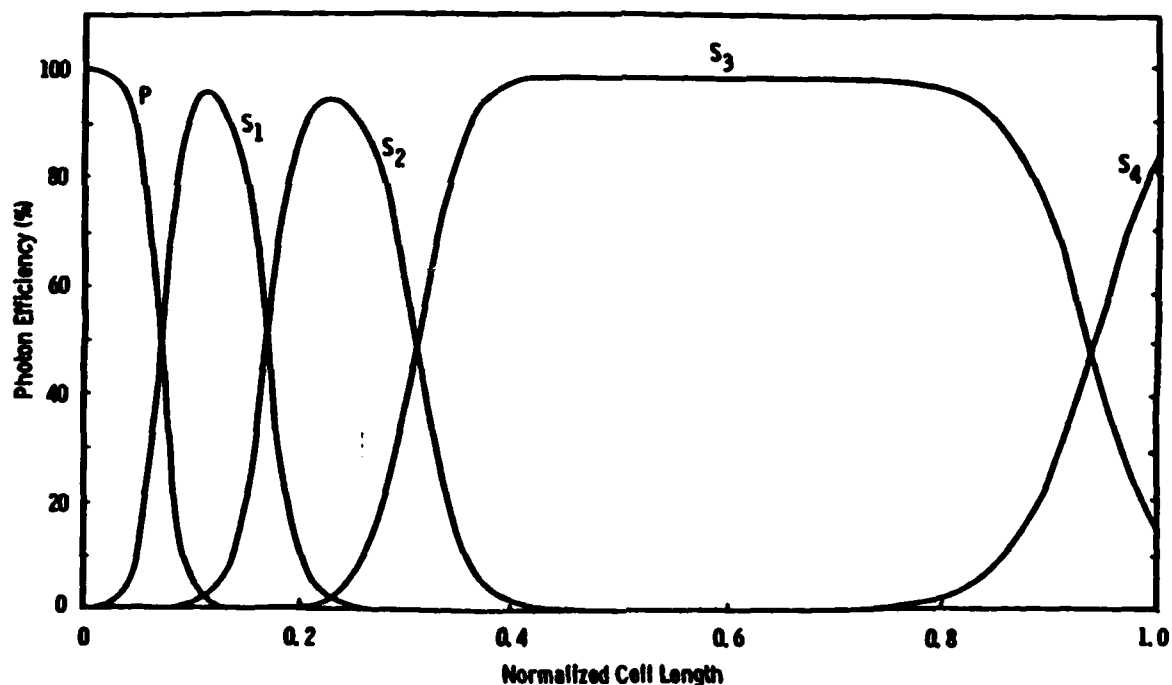


FIGURE 2. THIRD-ORDER RAMAN AMPLIFIER
PHOTON EFFICIENCY VS AMPLIFIER
LENGTH (Computer Simulation)

The equations describing multiple order Raman amplifiers, computer simulations of those equations, and the dependence of the amplifier gain on laser bandwidth are discussed in detail in Section 3.2.

3.0 THEORETICAL ANALYSES AND EXPERIMENTS

Initial experiments aimed at demonstrating efficient ultraviolet to visible Raman conversion were performed with the third harmonic radiation of a Nd:YAG laser at 355 nm and hydrogen gas as the Raman medium. This series of experiments led to the first observation of efficient Stokes conversion into the second order in a single Raman amplifier. In parallel with the experiments an extensive analysis was carried out to investigate the dependence of pump laser spectral width on the amplifier performance and to develop a comprehensive computer model of a Raman amplifier for the generation of higher Stokes orders. The analysis enabled resolution of an anomalous behavior of Raman gain observed in the initial experiments. Furthermore, the theoretical results led to the concept of gain enhancement by temporal matching, which was experimentally verified to be a key technique for optimizing Raman gains in an amplifier.

In the second phase of the program, a discharge pumped XeCl laser system was utilized to demonstrate significant conversion into the third Stokes (blue-green). Based on the results of the first phase, the XeCl laser system was operated to provide narrow bandwidth output. Using this pump source Raman amplifier energy conversion efficiencies near 14 percent (corresponding to 20 to 25 percent peak power efficiency) have been obtained for the blue-green output.

In the third phase of the program, the theoretical analysis was extended to include nonlinear dispersion effects in broadband laser pumped Raman amplifiers. The following sections present the key findings of the program.

3.1 Experiments with Nd:YAG/Third Harmonic Pump

Raman conversion experiments with the third harmonic (355 nm) of a Nd:YAG laser were first proposed to study the feasibility of efficient higher Stokes order generation in a novel Raman oscillator-amplifier configuration. An experimental schematic

is shown in Figure 3, in which the uv pump is the Nd:YAG third harmonic radiation with pulse lengths of 6 to 7 nanoseconds and an estimated bandwidth of 1.5 cm^{-1} .

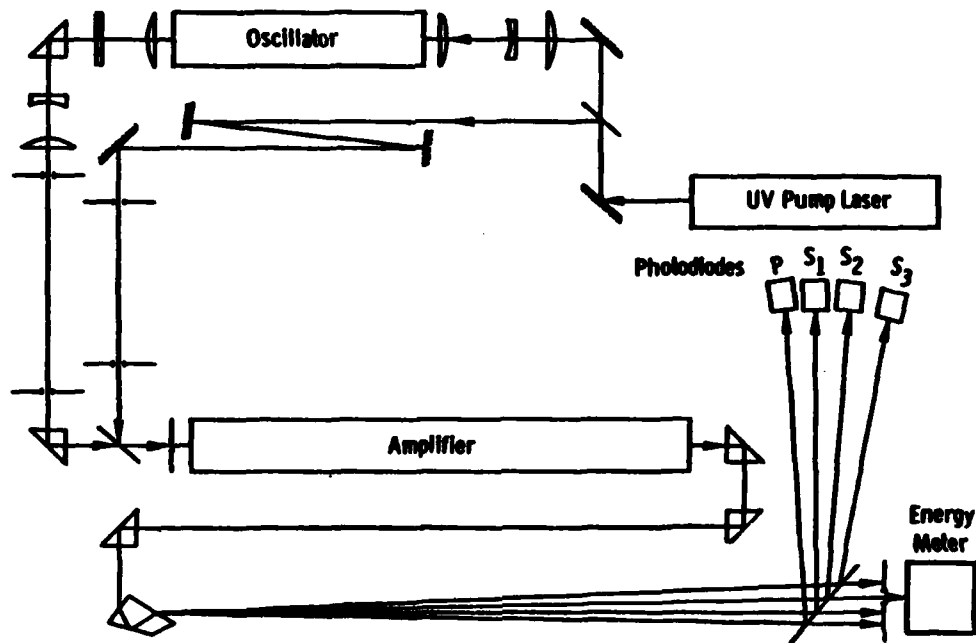


FIGURE 3. MULTIPLE STOKES RAMAN OSCILLATOR-AMPLIFIER EXPERIMENTAL LAYOUT

The 1 m long Raman oscillator cell was filled with 10 amagats of hydrogen gas at room temperature. A fraction of the pump beam was focused into the oscillator cell at power levels corresponding to several times the first Stokes stimulated emission threshold. Using a 2.5 ± 0.5 mm diameter beam and a 50 cm focal length lens, the threshold was observed at pulse energies near 1.1 mJ (0.16 MW). At 5 times the threshold level the second and third Stokes output could be readily generated at high efficiencies as indicated in Figure 4. At this pump level the energy conversion efficiencies are 25%, 31%, and 10% for the first, second and third Stokes, respectively.

The Raman amplifier for generating the higher Stokes orders consisted of copropagating pump and injected Stokes beams which were

collimated and overlapped in a 2 m long cell filled with 10 amagats of hydrogen gas. The injected Stokes beams were obtained from the oscillator output through suitable filters to transmit only the successive orders up to the desired order. A set of spatial apertures provided proper beam size overlap at the beam combining dichroic mirror. A similar set of apertures was also used for the amplifier beam.

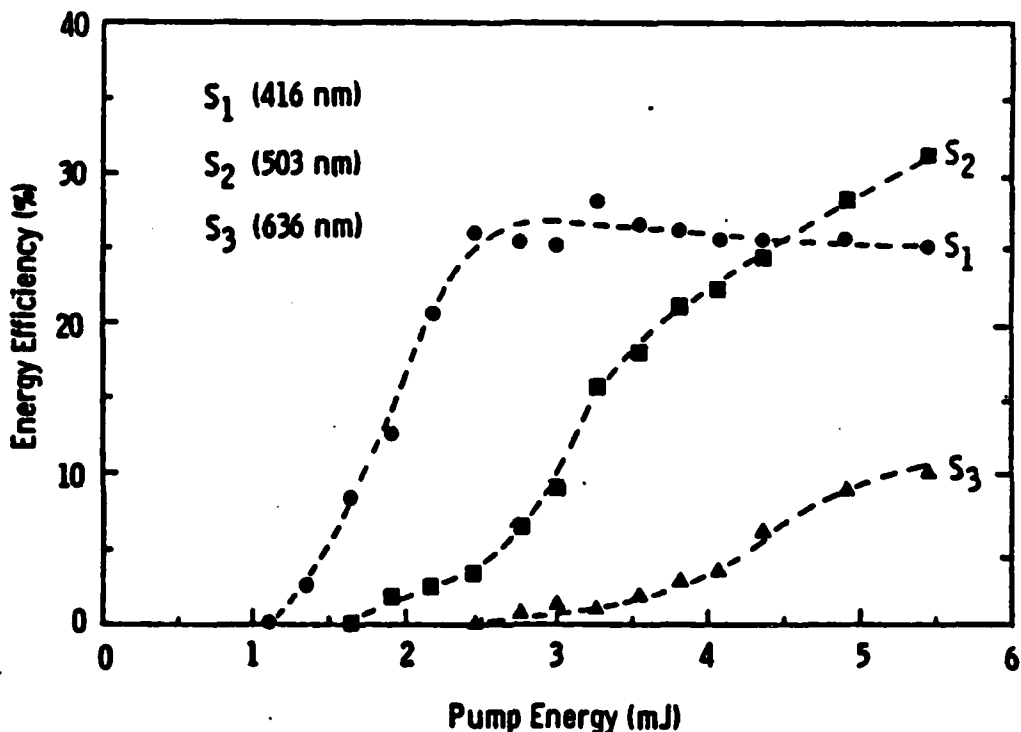


FIGURE 4. OSCILLATOR ENERGY CONVERSION EFFICIENCY vs PUMP ENERGY (P = 355 nm, H₂ @ 10 amagats)

In order to observe significant energy conversion into the Stokes orders, the overlapped beams were adjusted for angular alignment to within 0.1 milliradian. The observed beam divergence was approximately 0.3 milliradian which is smaller than the calculated four-wave mixing phase-matching angles near 3 milliradians. Indeed, under these alignment conditions a large fraction of the pump energy was converted into amplified Stokes radiation without significant four-wave mixing effects such as anti-Stokes generation.

To characterize the performance of the Raman amplifier, the pump energy was varied up to 9.5 mJ, a limit due to the apertured pump beam over a small filled-in portion of a unstable resonator mode. The injected Stokes energies were maintained at about several percent of the pump level. The pump and the first Stokes (S_1) pulses were roughly overlapped in time. Figure 5 shows the results of the amplifier energy conversion efficiency measurements for S_1 and S_2 as well as pump depletion data. According to the S_1 curve, a maximum of 50% energy conversion is achieved at pump energies near 7.5 mJ. At higher pump energies, the S_1 efficiency decreases at the expense of conversion into S_2 . The measured S_1 and S_2 energy efficiencies at 9.5 mJ are 38% and 20%, respectively, while the transmitted pump indicates 78% depletion.

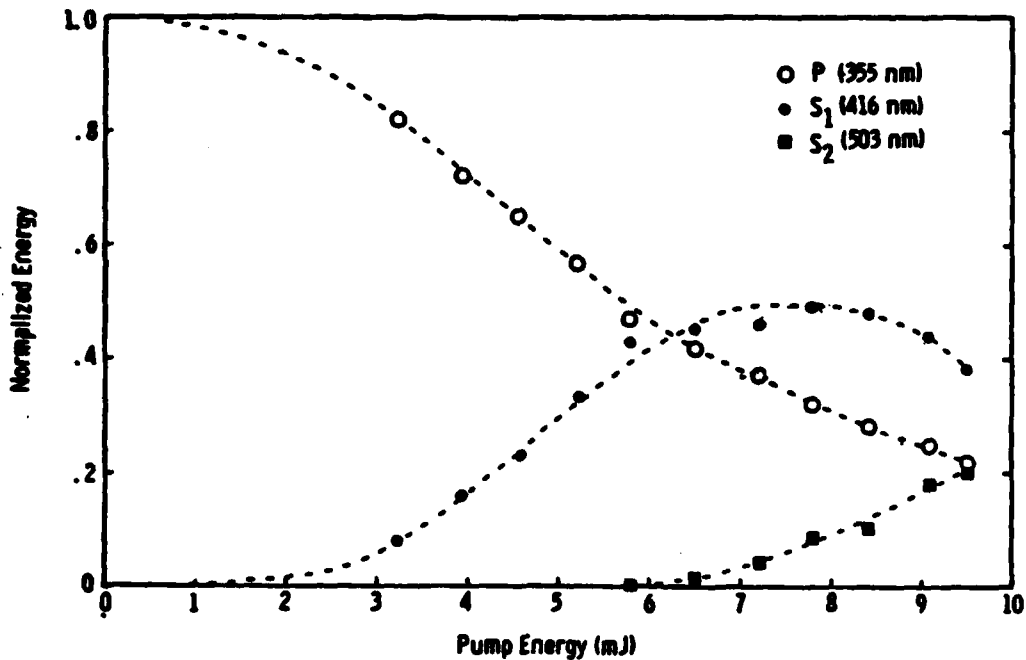


FIGURE 5. AMPLIFIER ENERGY CONVERSION vs PUMP ENERGY
(P = 355 nm, H₂ @ 10 amagats)

Pump depletion was also probed with fast silicon photodiodes to investigate further details of power conversion. Figure 6 represents oscillogram of 100 superimposed and time-correlated exposures taken at the 9.5 mJ pump level. The upper traces show the S_1 and S_2 pulses, and the lower traces are the pump pulses with (P') and without (P) the injected Stokes radiation. A complete power depletion is seen near the S_2 peak. The incomplete power depletion at the beginning and at the end of the pump pulse can be associated with smaller Raman gains due to less intense pumping and amplifier build-up time.

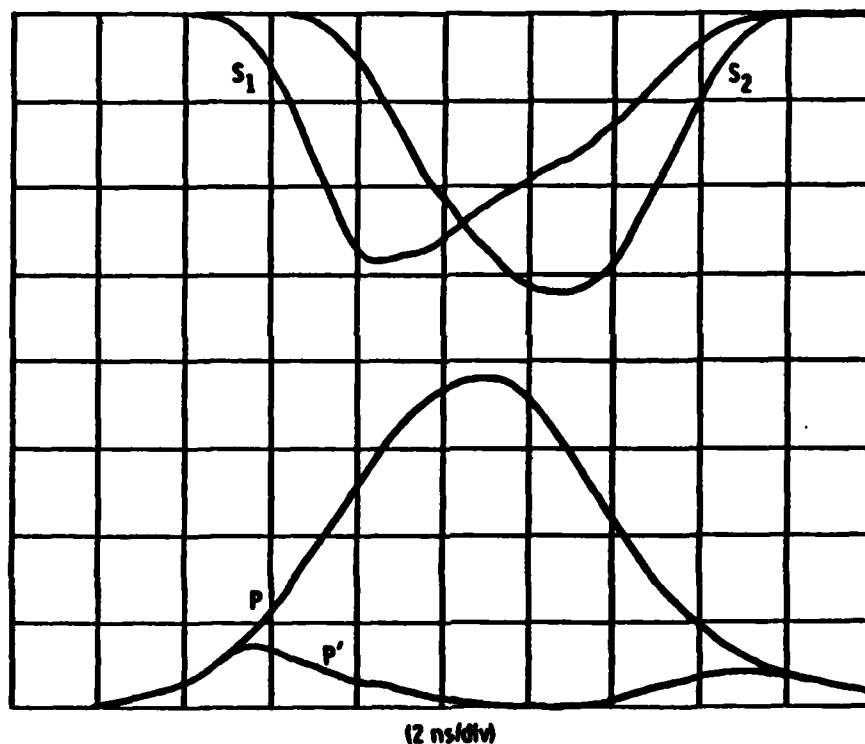


FIGURE 6. AMPLIFIED STOKES PULSES AND PUMP DEPLETION

In another series of experiments, the apertured amplifier pump beam was replaced by the annular unstable resonator mode with an outer diameter of approximately 4 mm. The data, shown in Figure 7, indicate a S_1 maximum energy efficiency of 58% near 10 mJ pump energy. At 20 mJ, the S_1 efficiency declines to 35%

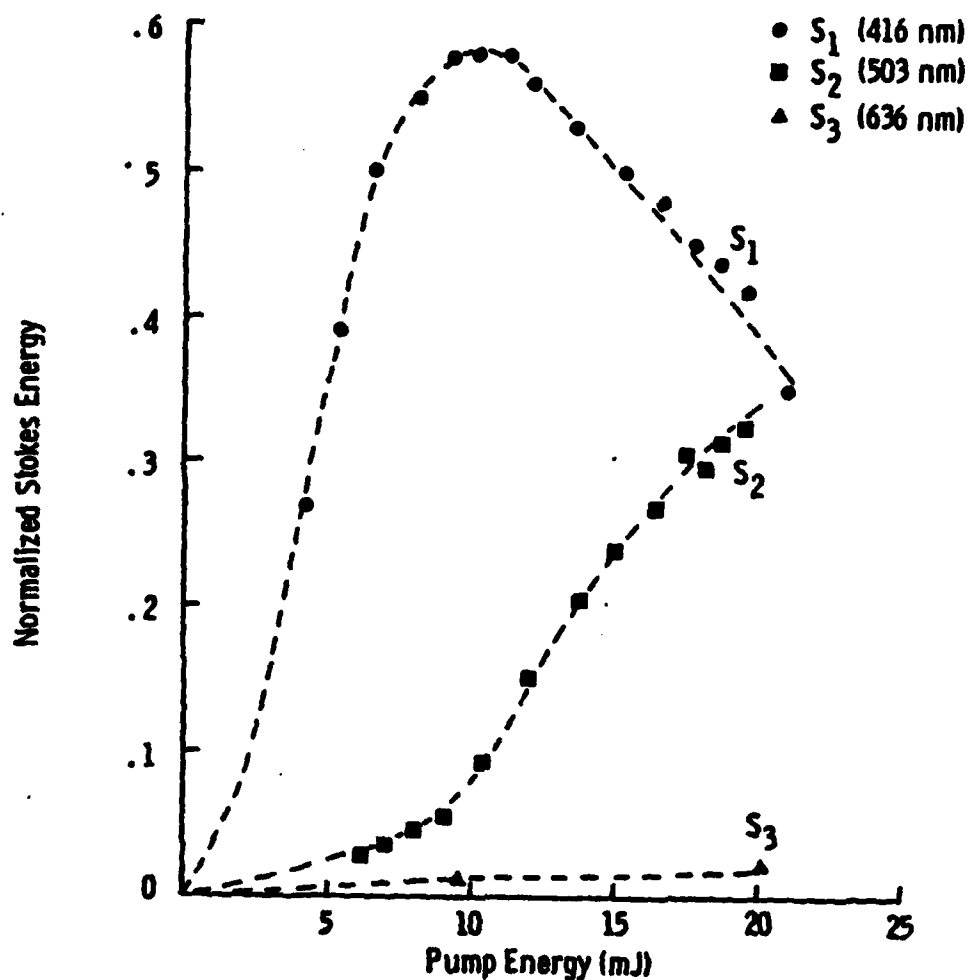


FIGURE 7. AMPLIFIER ENERGY CONVERSION
VS PUMP ENERGY
(P = 355 nm, H₂ @ 10 amagats)

but an S₂ efficiency of 35% is achieved. These results indicate that high conversion efficiencies should be possible using the unstable resonator output of the XeCl laser.

During measurement of Raman gain as a function of pump energy a nonexponential behavior was observed. The usual gains become evident only after the pump energy exceeds a certain amount. Figure 8 shows the first Stokes gain versus pump energy illustrating this behavior. For pump energies above 2 mJ, the amplification is exponential and shows gradually reduced gain above 4 mJ due to pump depletion. The nonexponential gains near 2 mJ level

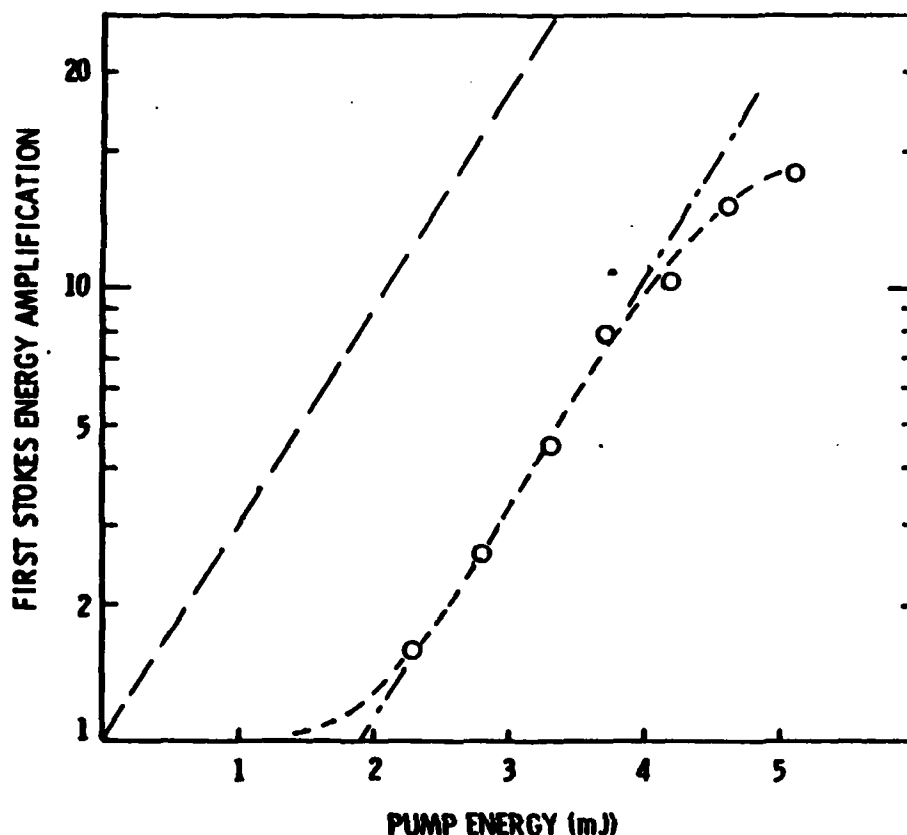


FIGURE 8. RAMAN GAINS VS PUMP ENERGY FOR
 A BROADBAND PUMP LASER
 $(\lambda_p = 355 \text{ nm}, \lambda_s = 416 \text{ nm},$
 $E_s(0)/E_p(0) \approx 2.5\%, \text{ H}_2 \text{ gas at}$
 $10 \text{ amagats})$

has now been identified to be a result of initially uncorrelated phases of the injected Stokes waves with respect to the pump wave at the entrance of the amplifier. This phenomenon is related to the spectral bandwidth of the pump laser. The theoretical details have now been analyzed and are presented in the next section.

3.2 Raman Amplifier Analysis

The analysis of Raman amplification of injected Stokes radiation was performed in two parts. The first part examined the effects

of broadband pumping on the gain and statistics of a single-order Raman amplifier. This effort was supplemented by an experiment to confirm some aspects of the analysis. The second part developed a model for calculating the successive buildup of higher Stokes orders in a multiple-order Raman amplifier pumped by a monochromatic source. The key results of the analyses are presented in the following sections.

3.2.1 Broadband Raman Scattering

The experiments of multiple-order Raman conversion described in Section 3.1 led to two observations which could not be explained using the conventional theory of Raman scattering of a monochromatic pump. First, the gain in a forward Raman amplifier was not proportional to the pump intensity as the theory would predict, but displayed a definite threshold intensity followed by a linear increase. Second, the relative shot-to-shot intensity fluctuations of the amplified Stokes pulse were greater than those of the pump, indicating a random variation in the Raman gain. The explanation of these apparent anomalies lies in the broadband character of the pump radiation. In order to understand the experimental data and to make accurate predictions of the performance of a practical frequency converter, a theory for Raman scattering of a nonmonochromatic pump radiation was developed. Experimental confirmation of one aspect of this theory is discussed in Section 3.2.2.

In order to analyze Raman scattering of a nonmonochromatic pump radiation, the pump and Stokes fields have been assumed to be plane waves which are represented by a summation over longitudinal cavity modes, i.e.:

$$\begin{aligned}
 E(z,t) = \frac{1}{2} \sum_m \left\{ u_m \exp i \left[(\omega_L + m\gamma) t - k_m^L z \right] \right. \\
 \left. + v_m \exp i \left[(\omega_L + m\gamma - \Omega) t - k_m^S z \right] \right\} + c.c.
 \end{aligned}
 \tag{1}$$

where γ is the mode spacing and u_m, v_m are the amplitudes of the individual laser (L) and Stokes (S) modes, respectively. Ω is the Raman shift (with homogeneously broadened linewidth Γ) and k 's represent the wave vector component in the direction of propagation.

Using the field expression (1), a system of equations for Raman scattering neglecting pump depletion is given by

$$\frac{\partial v_j}{\partial z} = \frac{g}{2} \sum_n \sum_m \frac{v_m u_{m-n}^* u_{j-n}}{1 + i \frac{2n\gamma}{\Gamma}} \exp[i(m-j)\gamma v z] \quad (2)$$

$$\frac{\partial u_j}{\partial z} = -\frac{g}{2} \sum_n \sum_m \frac{u_m v_{m-n}^* v_{j-n}}{1 + i \frac{2n\gamma}{\Gamma}} \exp[i(j-m)\gamma v z] \quad (3)$$

where g is the monochromatic power gain coefficient and $v = (1/c_L - 1/c_S)$ is the difference in reciprocal group velocities of the laser and Stokes waves. These equations take into account the slowly varying molecular displacement and are thus applicable to both transient and quasistatic Raman scattering. The amplitudes have been normalized such that $\bar{I}_{L0} = \sum_m |u_m|^2$ is the average laser intensity.

The effects of dispersion are contained in the exponential factors in the above equations. However, when the Raman gain in one coherence length is large, i.e.,

$$g\bar{I}_{L0} > \Delta\omega_L v \quad (\Delta\omega_L = \text{laser bandwidth}) \quad (4)$$

dispersion can be neglected. This criterion is satisfied in all of our experiments.

The solution of Equations (2) and (3) in the resonant regime ($\gamma \gg \Gamma$) and also in the transient regime ($\Delta\omega_L \gg \Gamma$) with uncorrelated pump modes is given by

$$\bar{I}_S(z) = \bar{I}_S(0) + \frac{1}{\bar{I}_{L0}} \sum_m |u_m^* v_m|^2_{z=0} \left[\exp(g\bar{I}_{L0}z) - 1 \right] \quad (5)$$

where \bar{I}_S is the time averaged Stokes intensity. Only the component of the Stokes wave which is proportional to the pump is amplified and it sees the monochromatic gain, $G = g\bar{I}_{L0}$.

For pump and Stokes spectra consisting of M modes with initially uncorrelated phases, Equation (5) reduces to

$$I_S(z) = I_S(0) \left\{ 1 + \frac{1}{M} [\exp(Gz) - 1] \right\}. \quad (6)$$

This function is plotted in Figure 9 for several values of M. Notice the similarity between these curves and the experimental data of Figure 8. The physical basis of the behavior of these curves can be understood as a phase correlation (or locking) process during Raman amplification. As the number of modes increases (i.e., degree of initial phase correlation decreases) the interaction length becomes longer to reach the same amplification.

In the general case without dispersion, the incremental forward gain is given by

$$G_f = \frac{g}{\sum_m |v_m|^2} \sum_n \frac{|\sum_m u_{m-n}^* v_m|^2}{(1 + i \frac{2n\gamma}{\Gamma})} \quad (7)$$

which depends on a correlation between complex amplitudes of the pump and Stokes modes. Since the phases of the pump modes are random, Equation (7) indicates shot-to-shot statistical fluctuations of the amplifier gain. These fluctuations are minimized for Stokes spectra which are proportional to the pump spectrum. This condition also yields the maximum gain which approaches the monochromatic value at large bandwidths ($\Delta\omega_L \gg \Gamma$). These results have been used as the basis for a gain enhancement technique which will be described next.

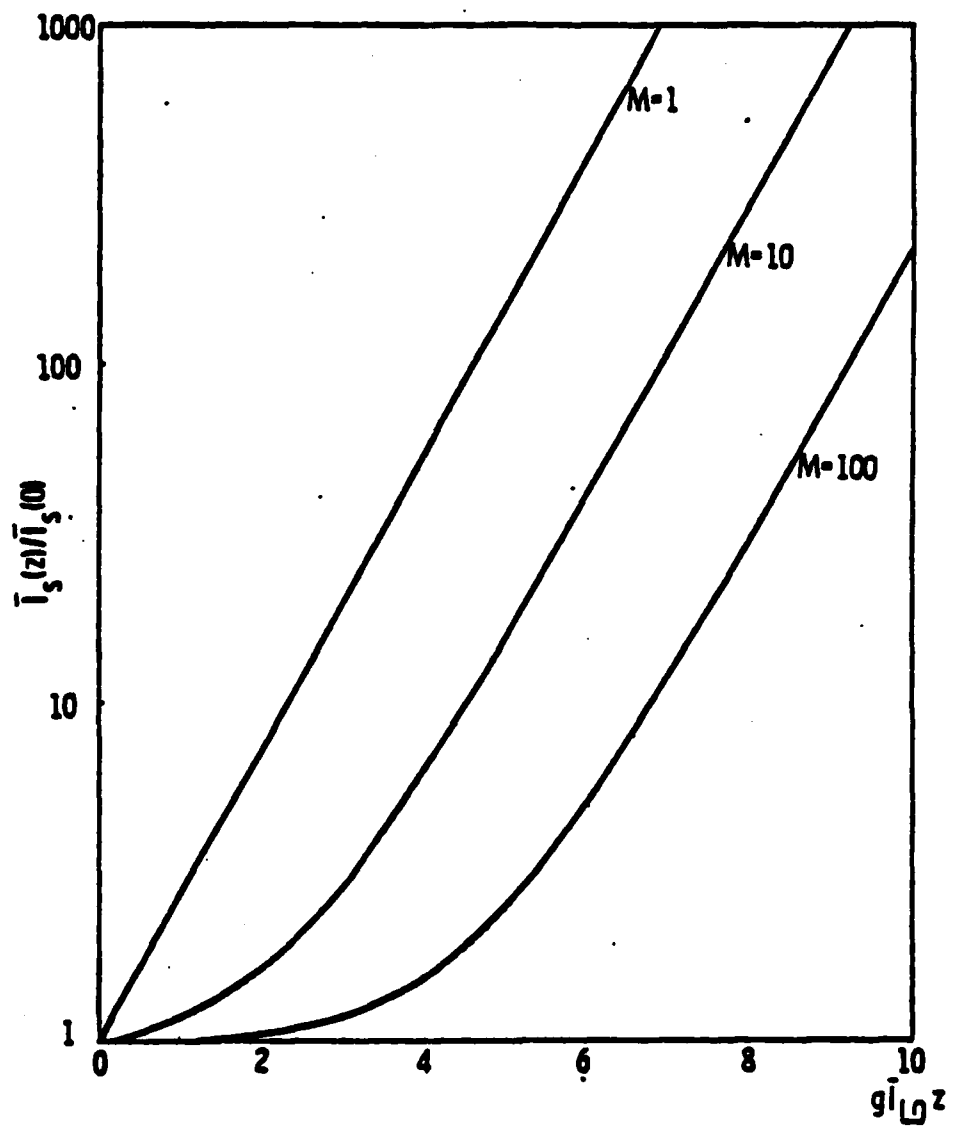


FIGURE 9 LASER-BANDWIDTH DEPENDENCE OF FORWARD GAIN IN A RAMAN AMPLIFIER WITH UNCORRELATED INJECTED PHASES

3.2.2 Gain Enhancement by Temporal Matching

In the theoretical analysis of a Raman amplifier pumped by a broadband pump laser it was shown that the Stokes wave experiences nonexponential gains in the initial part of the amplifier due to uncorrelated phases of the Stokes modes with respect to the pump modes. As the Stokes phases adjust themselves through amplification the differences for corresponding pump and Stokes modes approach some common value; thereafter, the gain rapidly reaches the monochromatic value. In the time domain, the optimum phase relationship corresponds to a Stokes waveform which is proportional to the pump waveform. It is therefore not unreasonable to expect that near-monochromatic gains may also be realized in Raman amplifiers, if the corresponding temporal fine structure of the injected pump and Stokes waveforms are superimposed at the entrance of the amplifier. We have experimentally investigated this gain enhancement by temporal matching, and the results verifying our analytical predictions are discussed below.

The experiment to test the effect of temporal matching in a Raman amplifier used a setup shown in Figure 10. It consists of a frequency doubled Quanta Ray Nd:YAG laser, two Raman cells with 20 amagats of hydrogen gas, a motor-driven optical delay, and detection equipment. The bandwidth of the 532 nm radiation could be selected as either 0.86 cm^{-1} or 0.33 cm^{-1} . The laser pulse length was 8 ns. Instead of using the full unstable beam profile, two nearly uniform beams were prepared for the oscillator and amplifier arms using apertures with a diameter of 3 mm. The Stokes pulses were detected with a PIN photodiode and either displayed on an oscilloscope screen or processed in a PAR box-car integrator and recorded with a chart recorder. Figure 11 shows two typical scans of amplified Stokes signal versus optical delay, one with and one without the etalon. Also shown is the unamplified injection Stokes signal. Care was taken in these experiments to attenuate the injected Stokes radiation at 683 nm sufficiently to prevent saturation in the amplifier.

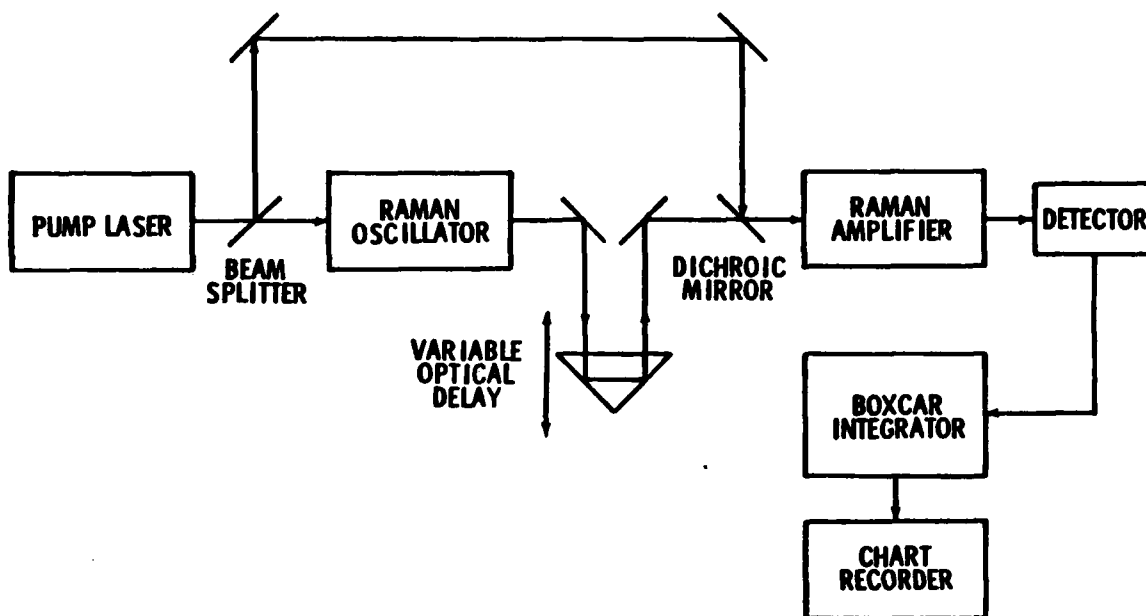


FIGURE 10. SCHEMATIC OF THE TEMPORAL MATCHING EXPERIMENT

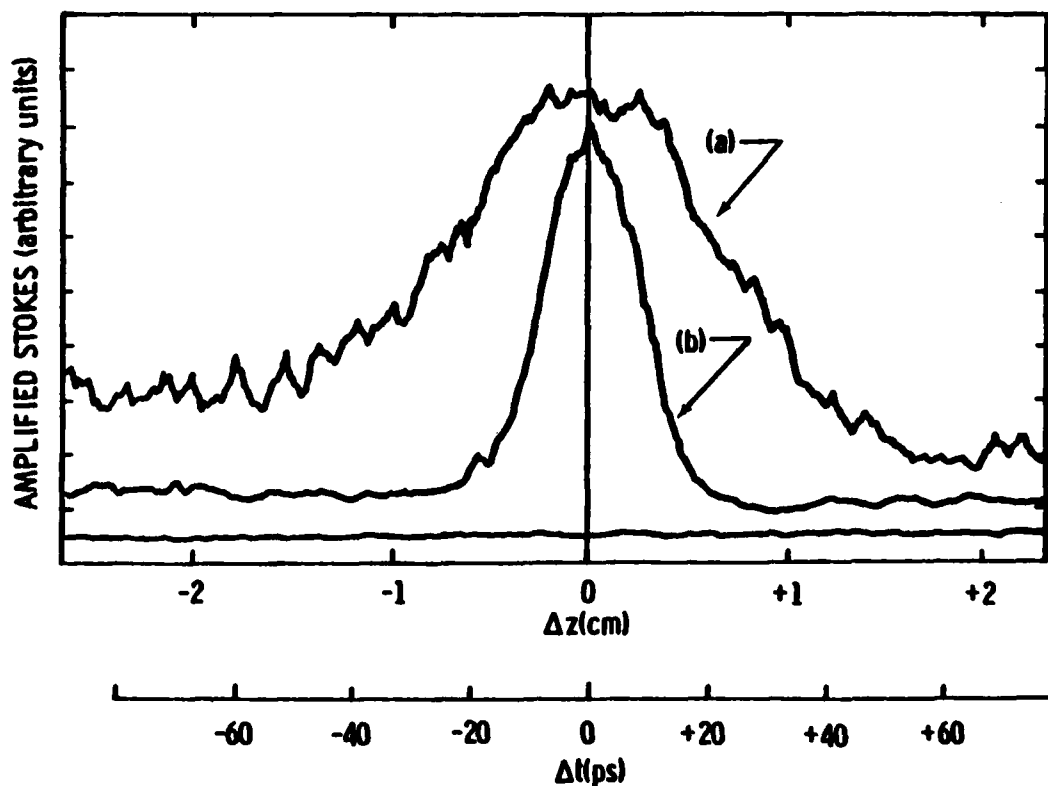


FIGURE 11. AMPLIFIED STOKES ENERGY VS OPTICAL DELAY FOR a) 0.33 cm^{-1} AND b) 0.86 cm^{-1} PUMP BANDWIDTH. (Position delays correspond to the pump preceding the Stokes; pump energy = 3 mJ; the baseline corresponds to the injected Stokes level.)

Several important observations can be made about the results. First, a substantial gain increase is observed as the pump and Stokes waveforms are scanned into coincidence. Second, the peak gain is the same with and without the etalon. Third, the width is narrower without the etalon, scaling roughly as the inverse of the pump bandwidth. Finally, the curves are asymmetric with higher gains observed when the Stokes pulse precedes the pump. Unfortunately, it is not possible to derive an exact analytical expression for the amplification versus relative delay for the conditions of the present experiment. However, for a broadband noise pump with a rectangular spectrum and when the incident pump and Stokes waveforms are proportional, except for a relative delay Δt , the amplified Stokes in the small signal regime is given by:

$$I_S(\xi) = I_S(0) \left[1 + \frac{\text{sinc}^2\left(\frac{\Delta\omega_L \Delta t}{2}\right)}{\text{sinc}^2\left(\frac{\gamma \Delta t}{2}\right)} (e^\xi - 1) \right] \quad (8)$$

where $\Delta\omega_L$ is the laser bandwidth. This function is periodic with a period equal to the laser round trip time, and the widths of the major peaks are inversely proportional to the laser bandwidth, i.e.

$$\Delta t_{\frac{1}{2}} = 5.57/\Delta\omega_L . \quad (9)$$

The values of $\Delta t_{\frac{1}{2}}$ from Equation (9) using the known laser bandwidths agree well with the widths as seen in Figure 11. In the present experiment it was not possible to measure the periodicity because of the short pulse length. Figure 12 summarizes the results of a number of measurements at different pump energies. Shown are the gains on and off the peak, with and without the etalon. On a semilogarithmic graph, for gains not too close to unity, the measured data can be fitted well with parallel straight lines. The most important feature to notice is that the peak gains are located on a line going approximately through the

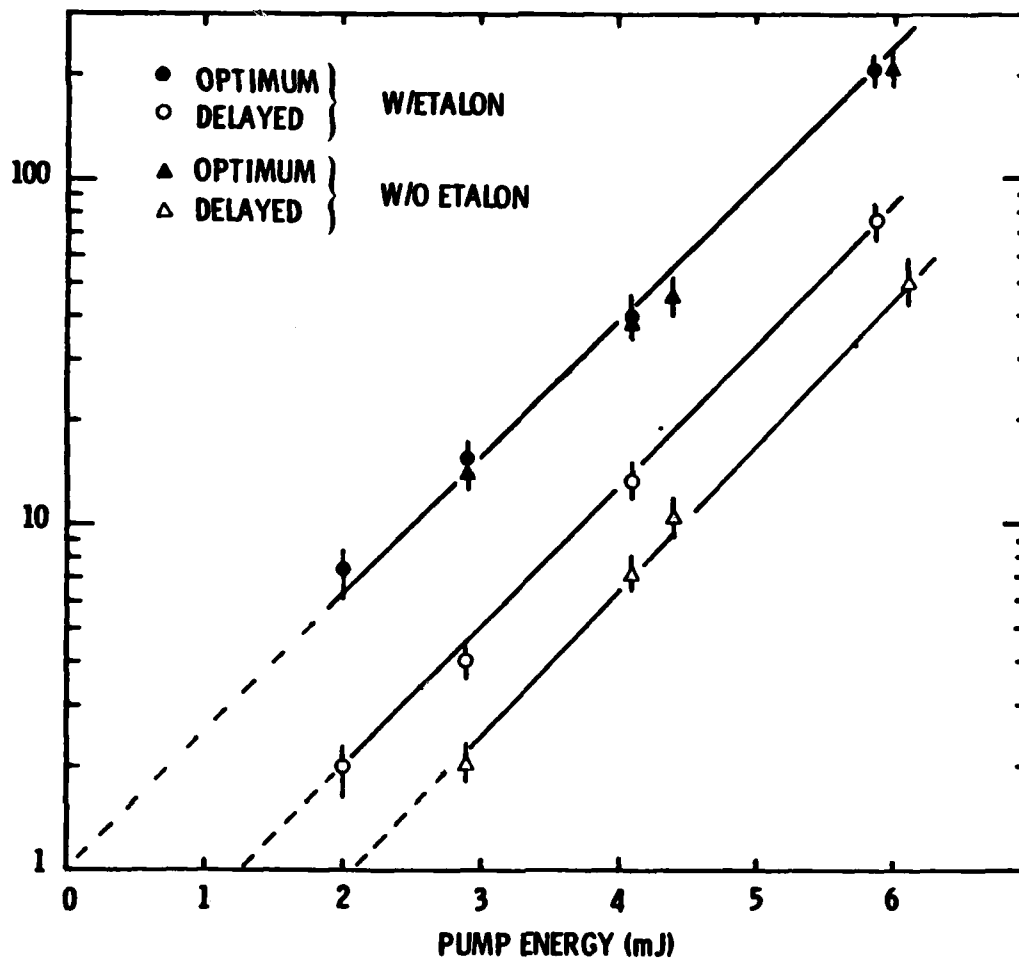


FIGURE 12. RAMAN AMPLIFIER GAIN VS PUMP ENERGY

origin, as would be the case for an oscillator. This fact, combined with absolute gain estimates, indicates that the measured peak gains are close to the monochromatic values. Therefore, the temporal matching technique should make it possible to use Raman amplifiers without having to narrow the laser spectrum to near monochromatic conditions. It should be noted, however, that the amplified Stokes spectrum retains the pump spectrum under this gain enhancement technique.

One additional feature of temporal matching is a significant reduction in the gain fluctuation as the pump and the Stokes waveforms are brought into coincidence. Depending on the pump

laser bandwidth, this property may help to control fluctuations in the higher Stokes order efficiency due to gain fluctuations.

In summary, the importance of phase correlation in a Raman amplifier has been clearly established by the theoretical analysis of broadband pumping and by the experimental demonstration of the gain enhancement technique. To make use of this technique for practical systems, laser bandwidths less than 1 cm^{-1} are preferable from temporal alignment considerations.

3.2.3 Raman Amplifier Computer Simulation

The analysis on the effect of pump bandwidth on Raman amplifier gain showed that the gain is maximized by either using a monochromatic pump laser or utilizing the gain enhancement technique. In either case the Stokes waves experience the monochromatic gains. Therefore, we have analyzed a multiple-order Raman amplifier pumped by a monochromatic source in order to model conversion processes and to predict efficiencies for the various Stokes orders.

The steady-state equations describing the interaction of the various Stokes and anti-Stokes orders are compactly written as:

$$\frac{dE_n}{dz} = -i\gamma\bar{\omega}_n \left[q^* E_{n+1} e^{ik_{n+1}z} + q E_{n-1} e^{ik_{n-1}z} \right] e^{-ik_n z} \quad (10a)$$

$$q = -i\beta \sum_m E_{m-1} e^{i(k_{m-1})z} \quad (10b)$$

where:

- E_n = Complex Field Amplitude
- n = Order Index $\begin{cases} n = 0 \text{ Pump} \\ n < 0 \text{ Stokes} \\ n > 0 \text{ Anti-Stokes} \end{cases}$
- $\bar{\omega}_n$ = Normalized Frequency $= \omega_n / \omega_{-1}$
- k_n = Wave Vector

q = Molecular Vibration Amplitude

γ, β = Coupling Coefficients

These equations are then solved numerically on a computer to simulate amplification of the Stokes orders under a set of prescribed initial conditions. The characteristic parameters used are the first Stokes gain, G , and the relative intensities of the injected Stokes radiation normalized to the pump intensity.

Figures 13 and 14 are two examples of power conversion versus gain in a H_2 Raman amplifier pumped by a XeCl laser. The injected Stokes intensities are one percent for the first three orders and 10^{-2} percent and 10^{-4} percent for the fourth order in Figures 13 and 14, respectively. The effect of suppressing the fourth order injection is significant in extending the gain values for which the third Stokes is maximized.

In the simulation runs, a rectangular beam profile and pulse shape were assumed. However, the code can also be used to simulate nonuniform beam profiles and pulse shapes. As an example, a model calculation of the energy conversion efficiencies was performed for the case of 355 nm pumped second order amplifier. The injection intensities have been chosen from experimental data, and uniform beam profile and Gaussian pulse shape were assumed to approximate the actual experimental conditions. Figure 15 gives the results which show a good agreement with the data in Figure 5 of Section 3.1. It should be noted that the scale of amplifier gain is not the same in the two figures. This discrepancy is due to the reduced gains in the experiment resulting from initially uncorrelated phases of the pump and Stokes modes at the amplifier entrance.

For nonuniform beam profiles the code can be used to predict spatially integrated conversion efficiencies for cases in which

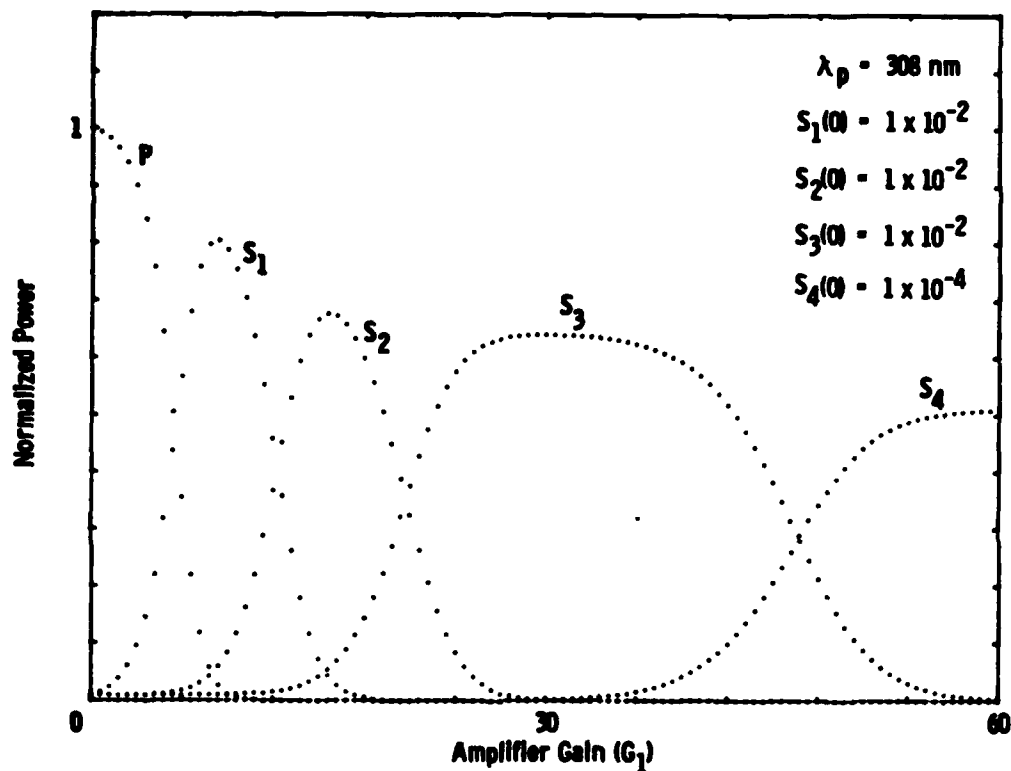


FIGURE 13. H₂ RAMAN AMPLIFIER POWER CONVERSION VS GAIN FOR UNIFORM BEAM PROFILE

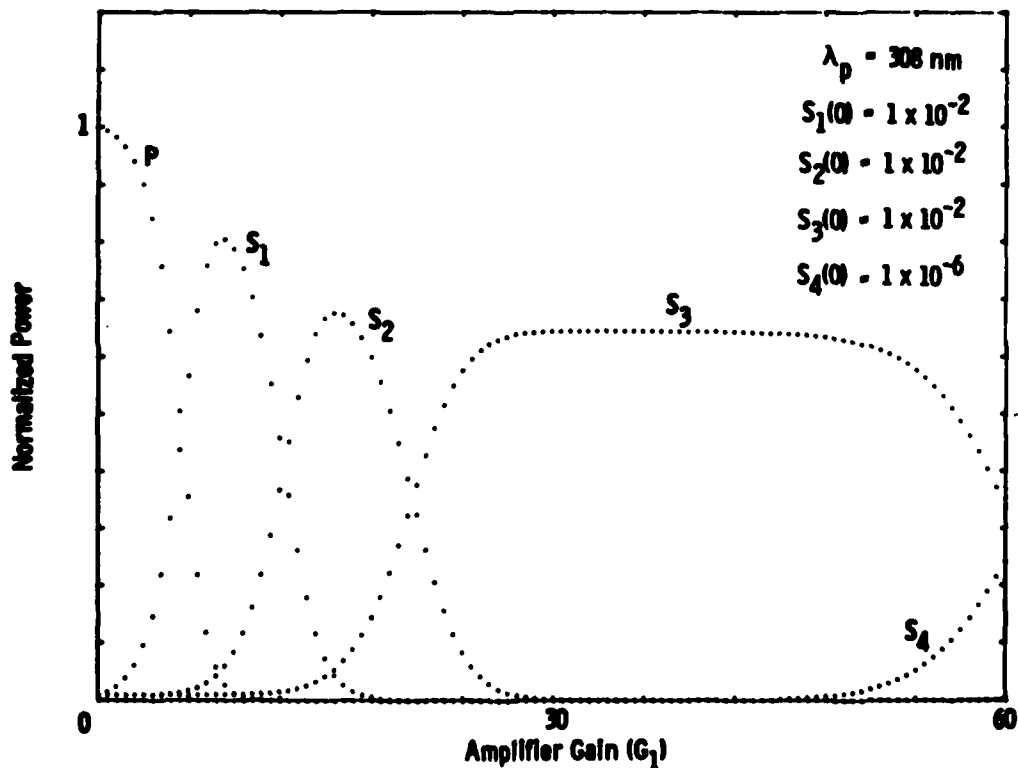


FIGURE 14. H₂ RAMAN AMPLIFIER POWER CONVERSION VS GAIN FOR UNIFORM BEAM PROFILE

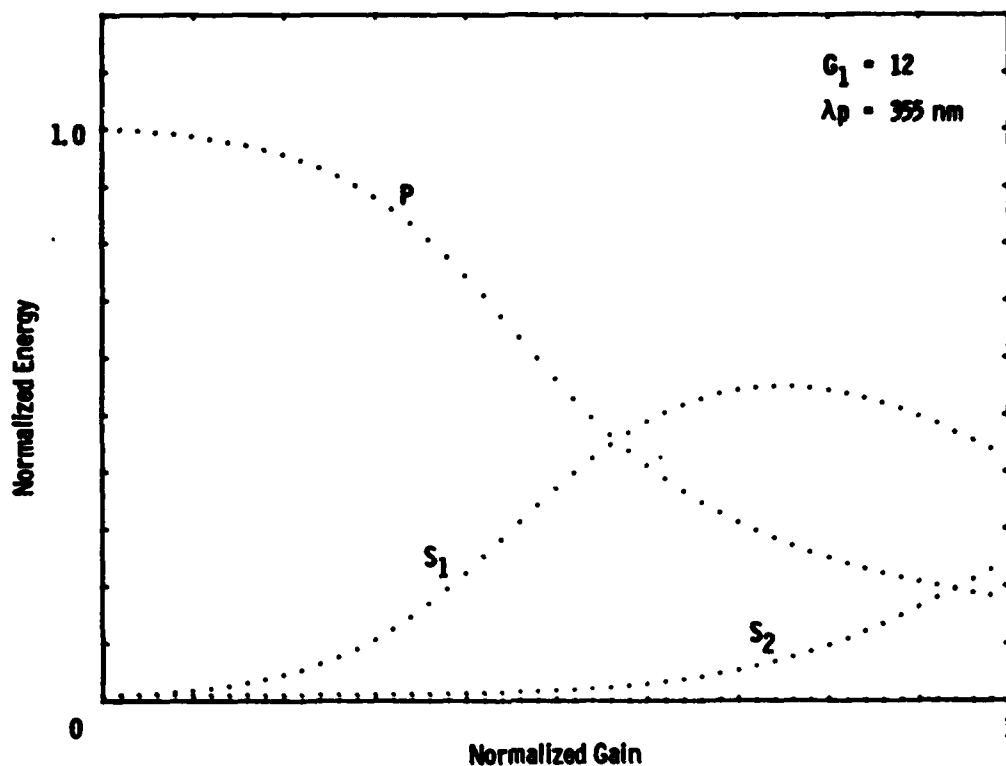


FIGURE 15. RAMAN AMPLIFIER ENERGY CONVERSION VS GAIN IN H_2 : GAUSSIAN PULSE SIMULATION

the interaction length is small compared to the confocal parameter or an equivalent measure of collimation. Such calculations have been useful in the XeCl Raman conversion data analysis and are discussed in that section.

3.3 XeCl Laser Raman Conversion

The main purpose of the second phase of the program was to demonstrate XeCl laser Raman conversion, using the oscillator-amplifier system. In particular a major effort was devoted to constructing a suitable pump laser system which is capable of achieving significant Raman conversion efficiencies for the the blue-green output. This section presents a description of an XeCl pump laser system and a discussion of the experimental data which have shown up to 14 percent blue-green energy conversion with respect to the pump energy in the Raman amplifier [KS82].

3.3.1 Narrow Bandwidth XeCl Laser System

From the discussion of laser bandwidth effects in Raman amplifiers, it is clear that a spectrally narrow XeCl pump laser is a suitable source for Raman conversion into higher Stokes outputs. In addition the beam quality and output power must be sufficiently high to permit efficient operation of the Raman oscillator-amplifier system. To satisfy these requirements, a commercial electric discharge pumped XeCl laser (Lambda-Physik EMG 100) was chosen. This laser is equipped with a 30-liter gas reservoir and a recirculation fan to permit repetitively-pulsed operation at up to 10 pps. The laser can produce ~ 2 W average power at 10 pps in ≤ 10 ns primary pulses when the cavity consists of a flat high reflector and a flat uncoated CaF_2 output coupler. However, the beam quality is far from being adequate. Thus, our approach was to use the laser as an XeCl amplifier with an injection source at 308 nm having narrow spectral width and good beam quality.

The injection source was provided by the frequency doubled output of a narrow bandwidth pulsed dye laser system. An overall block diagram of the experimental configuration is shown in Figure 16. The dye laser system, which consists of an oscillator and two amplifiers, is pumped by the second harmonic of a Q-switched Nd:YAG laser as schematically shown in Figure 17. In order to generate narrow bandwidth output at 616 nm, a solid etalon is inserted in the dye oscillator. A Fabry-Perot interferometer measurement revealed a spectral width of approximately 0.2 cm^{-1} (0.08 \AA) for the main dye amplifier output. Based on this measurement the frequency doubled output is estimated to have a bandwidth of about 0.4 cm^{-1} (0.04 \AA) at 308 nm.

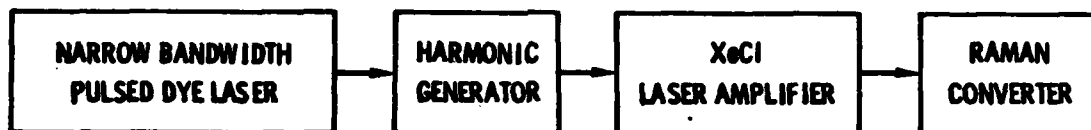


FIGURE 16. RAMAN CONVERSION OF XeCl LASER EXPERIMENTAL CONFIGURATION

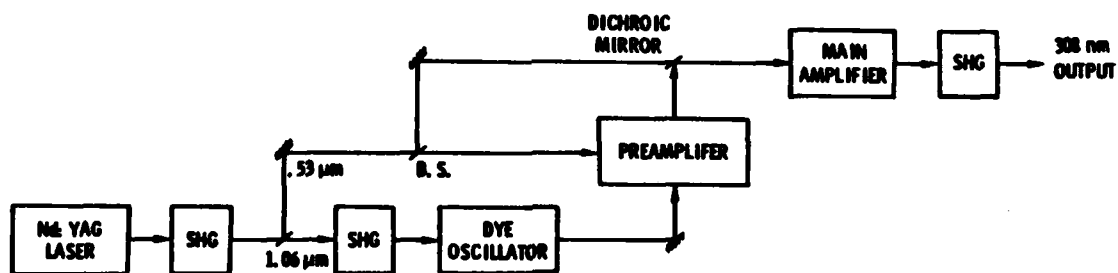


FIGURE 17. PULSED DYE OSCILLATOR-AMPLIFIER SYSTEM WITH SHG

The operation of the XeCl laser as a well behaved amplifier required a careful control of pulse timing and spatial extraction cross section. Since the primary excitation duration was the 8 ns injection pulses had to be time overlapped to within < 10 ns, a few nanoseconds for stable output. The best amplified beam quality was obtained when the injection beam was closely matched to the nearly rectangular (9 x 25 mm) discharge region in the laser. Under these conditions and using the manufacturer's recommended gas mixture (3-5% Xe, 0.3% HCl, balance Ar at 1.2 bar) pulse energies up to 20 mJ have been obtained. A different gas mixture (2% Xe, 0.2% HCl, balance He at 2.4 bar) gave output energies of about 35 mJ.

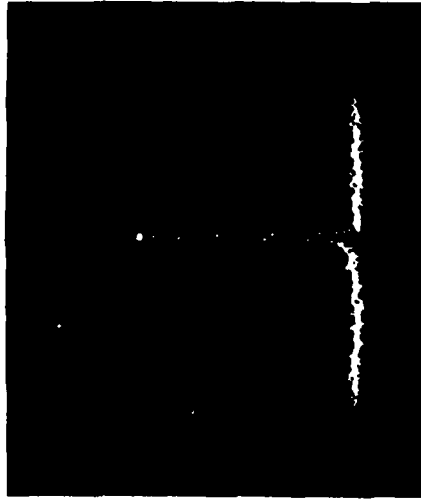
To determine the spectral property of the XeCl amplifier, a Spex 3/4 m spectrograph interfaced to a PAR optical multichannel analyzer (OMA) was used to record the laser spectrum with and without the injection beam. Figure 18(a) shows the typical XeCl spectrum, while Figure 18(b) indicates a narrow bandwidth output (instrument limited resolution) when the injection wavelength was tuned to the shorter wavelength peak (higher peak in Figure 18(a)). It should be noted that a neutral density filter was used to reduce the beam intensity substantially to obtain Figure 18(b). By tuning the injection wavelength across the XeCl spectrum, it was possible to tune the amplifier output continuously between the outer edges of the two main transition peaks of Figure 18(a) without competition from free-running oscillations.

3.3.2 Raman Oscillator-Amplifier System

The experimental layout of the Raman converter is illustrated in Figure 19. A photograph of the apparatus is also shown in Figure 20. To operate the oscillator-amplifier system the output of the XeCl laser amplifier is split into two beams: a fraction of the nearly rectangular beam is intercepted by a right angle prism to direct a pump beam into a Raman oscillator, and the



(a) Free-running Laser



(b) Narrow Bandwidth Amplifier

FIGURE 18 XeCl LASER/AMPLIFIER SPECTRUM

NORTHROP
Research and Technology Center

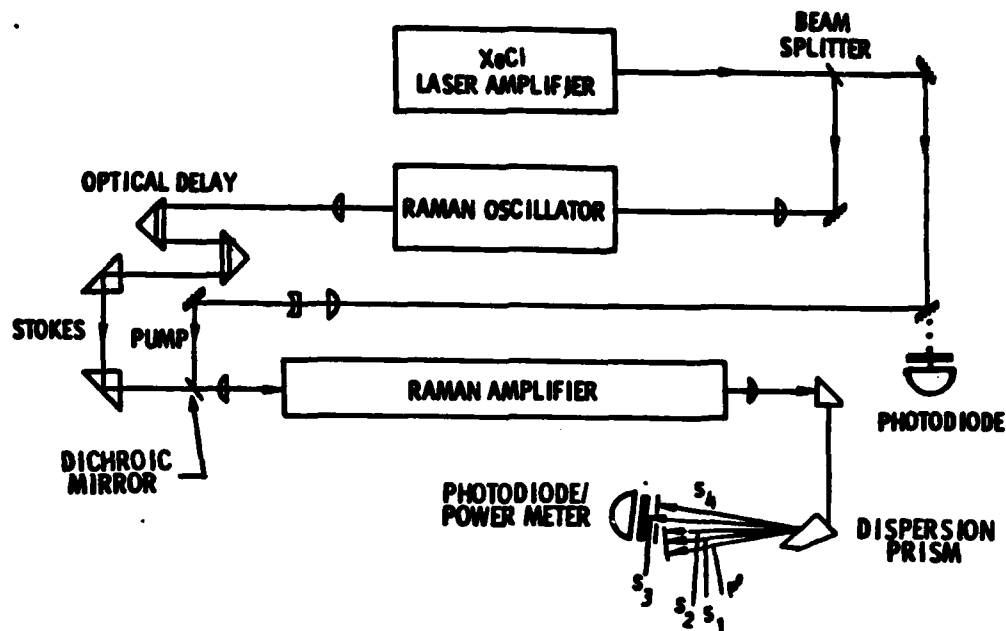


FIGURE 9. RAMAN CONVERTER CONFIGURATION

remaining beam is routed to pump a Raman amplifier. The performance characteristics of the oscillator and the amplifier are presented below.

The oscillator consists of a cell filled with hydrogen gas as Raman medium and a pair of lenses: one for focusing the pump beam inside the cell and the other for recollimating the Stokes output. To optimize the multiple Stokes output the cell pressure and focusing geometries were varied. For a 1 m focal length lens whose focal plane is located near the midpoint of the cell, pressures above 150 psig (> 10 atm) are found to increase the threshold for the higher Stokes orders while keeping the first Stokes threshold nearly constant.

At pressures below 100 psig (< 8 atm) the third Stokes threshold decreased significantly to allow efficient multiple Stokes generation. To obtain stable operation with three Stokes orders the oscillator was pumped with about 7 mJ which corresponded to approximately seven times the first Stokes threshold level. The fourth Stokes output as well as up to three anti-Stokes orders were observed, but their intensities were substantially lower than the first, second and third Stokes output. Due to

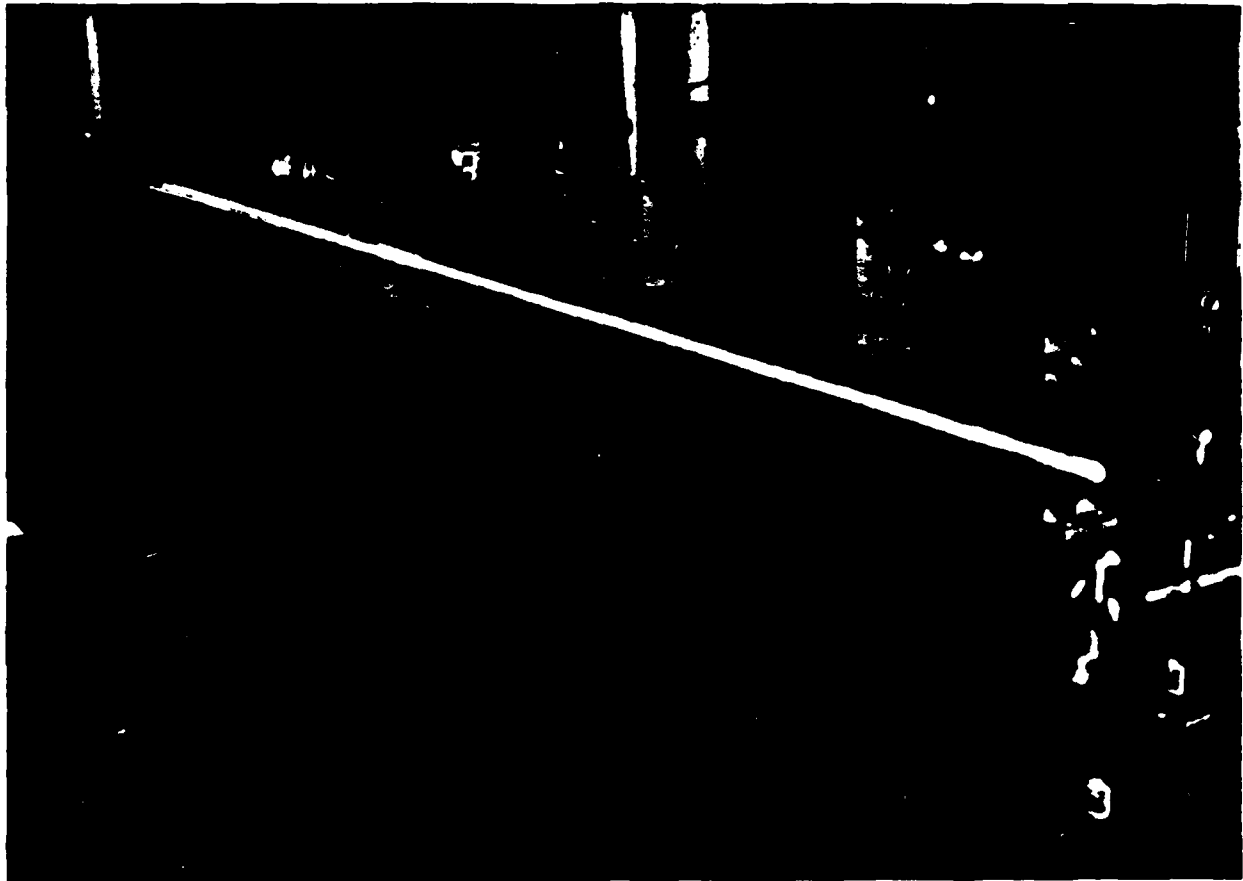


FIGURE 20. Photograph of Raman oscillator-amplifier setup showing Stokes beams after a dispersion prism. The third Stokes (blue-green 499 nm) beam is seen between the second Stokes (violet 414 nm) and the fourth Stokes (red 631 nm) beams.

the short pulse lengths used in this experiment a nominal working pressure near 80 psig (~ 6 atm) was chosen in order to minimize buildup times while maintaining efficient multiple Stokes generation. For longer pulses (> 20 ns) the oscillator should be able to operate at lower pressures (e.g. $2\sim 3$ atm) with threshold levels comparable to the present case, since the steady-state vibrational Raman threshold has been measured to be nearly constant above $2\sim 3$ atmospheres [TPB79].

The amplifier cell is made of a 2-m long stainless steel tubing with normal incidence windows at both ends. An uncoated fused silica window and an anti-reflection coated window (340 - 500 nm) are used at the amplifier input and output, respectively. The cell was filled with hydrogen gas to near 80 psig to match the oscillator cell.

To generate the blue-green output in the Raman amplifier the oscillator output and the amplifier pump beams are combined at a dichroic mirror as shown in Figure 19. This mirror is coated to reflect $> 99\%$ at 308 nm and transmit $> 80\%$ at the Stokes wavelengths of 353 nm (S_1), 414 nm (S_2), and 499 nm (S_3). Measurements of the Stokes beam energy in front of the amplifier indicated approximately 0.4 mJ (S_1), 0.45 mJ (S_2), 0.45 mJ (S_3), and 0.2 mJ (S_4).

Initial amplifier experiments were conducted with collimated pump and Stokes beams in the cell. This arrangement produced significant S_1 and S_2 output, but the S_3 (blue-green) conversion efficiency was on the order of one percent due to insufficient pump intensity of a 2.5 mm x 4 mm beam. Thus, a 1 m focal length lens was inserted in front of the amplifier input window to provide higher pump intensities in the cell. After overlapping the pump and injected Stokes beams to within 0.2 mrad, amplification of the third Stokes was readily observed. A further increase of the S_3 output was obtained when the optical delay (consisting of two offset opposing right angle prisms) was

adjusted for optimum temporal overlap of the Stokes pulses and the pump pulse as expected.

For the measurement of amplifier conversion efficiency as a function of pump energy, a recollimating lens was inserted after the cell and the Stokes beams were spatially separated by a dispersion prism. Using a Scientech Model 360001 power meter (with isoperibol enclosure) at appropriate locations, the pulse energy data were collected for each of the Stokes output. Figure 21 shows the conversion efficiency data for pump energies of up to 13.5 mJ inside the cell. The amplifier efficiency is defined here as the fraction of the pump energy which is converted into a given Stokes order in the amplifier. Depleted pump output (P') data are also included in Figure 21. According to the graph an S_3 energy conversion efficiency of 14 percent has been demonstrated with the focused pumping configuration in the amplifier.

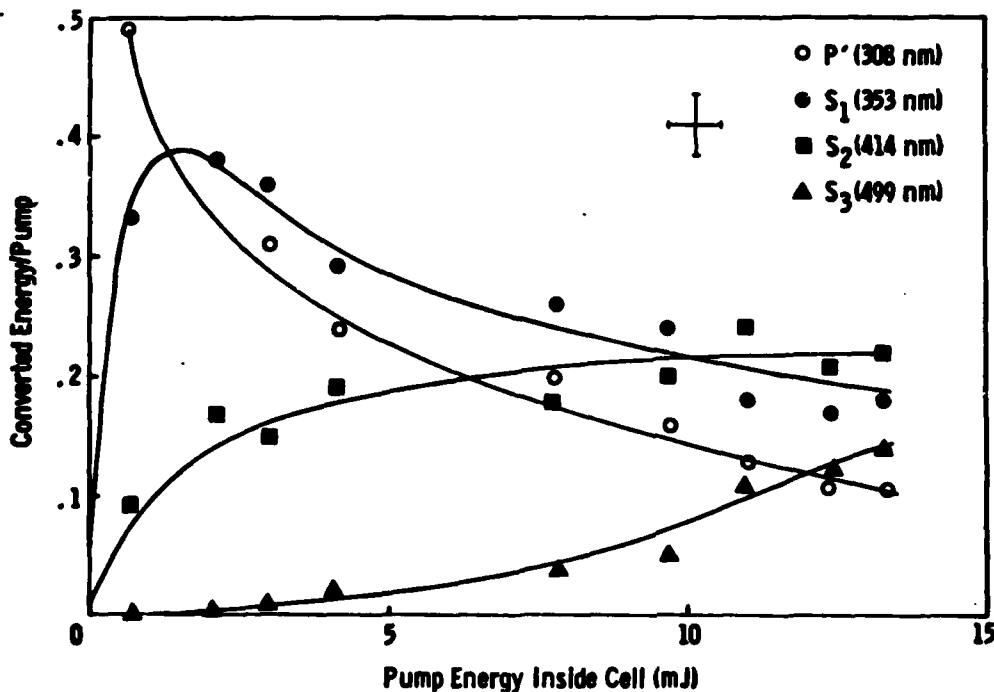


FIGURE 21. H_2 RAMAN AMPLIFIER ENERGY CONVERSION VS PUMP ENERGY

Figure 22 shows typical input pump and amplified S_3 pulse traces obtained with two ITT F4000 S1-UV photodiodes whose signals were added (with a time delay) on a Tektronix 7834 storage oscilloscope. Note that the S_3 pulse occurs after a few nanoseconds into the pump pulse due to buildup time. From these pulse length data, we estimate peak S_3 power conversion efficiencies in the range of 20 to 25 percent.

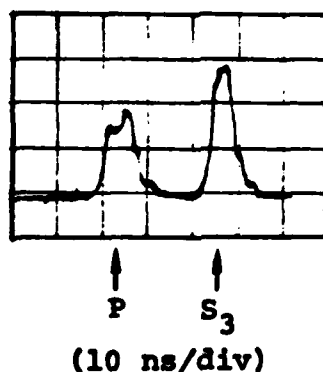


FIGURE 22. PUMP INPUT AND AMPLIFIED THIRD STOKES PULSES

The focused pumping configuration used in the current amplifier setup is not an optimum approach because of diffraction effects and four-wave mixing processes. First, the diffraction effects near the focal region can cause suboptimal beam overlap of the pump and the successive Stokes orders because of the widely different wavelengths. In particular, the energy in the central lobe of the focused pump beam is reduced and has a nonuniform radial distribution (e.g., Airy function). To illustrate this point, a computer simulation of amplifier power conversion efficiency as a function of gain is shown in Figure 23 for the case of a Gaussian beam profile. A comparison with the case of a uniform beam profile (see Figures 13 and 14) clearly indicates reduced efficiencies of the Gaussian beam profile. Second, the focusing of the beams can enhance four-wave mixing processes by angular phase-matching, which reduce the ultimate Raman amplifier conversion efficiencies. Indeed, these four-wave mixing processes were observed in the present experiment although their efficiencies are estimated to add up to about a few percent.

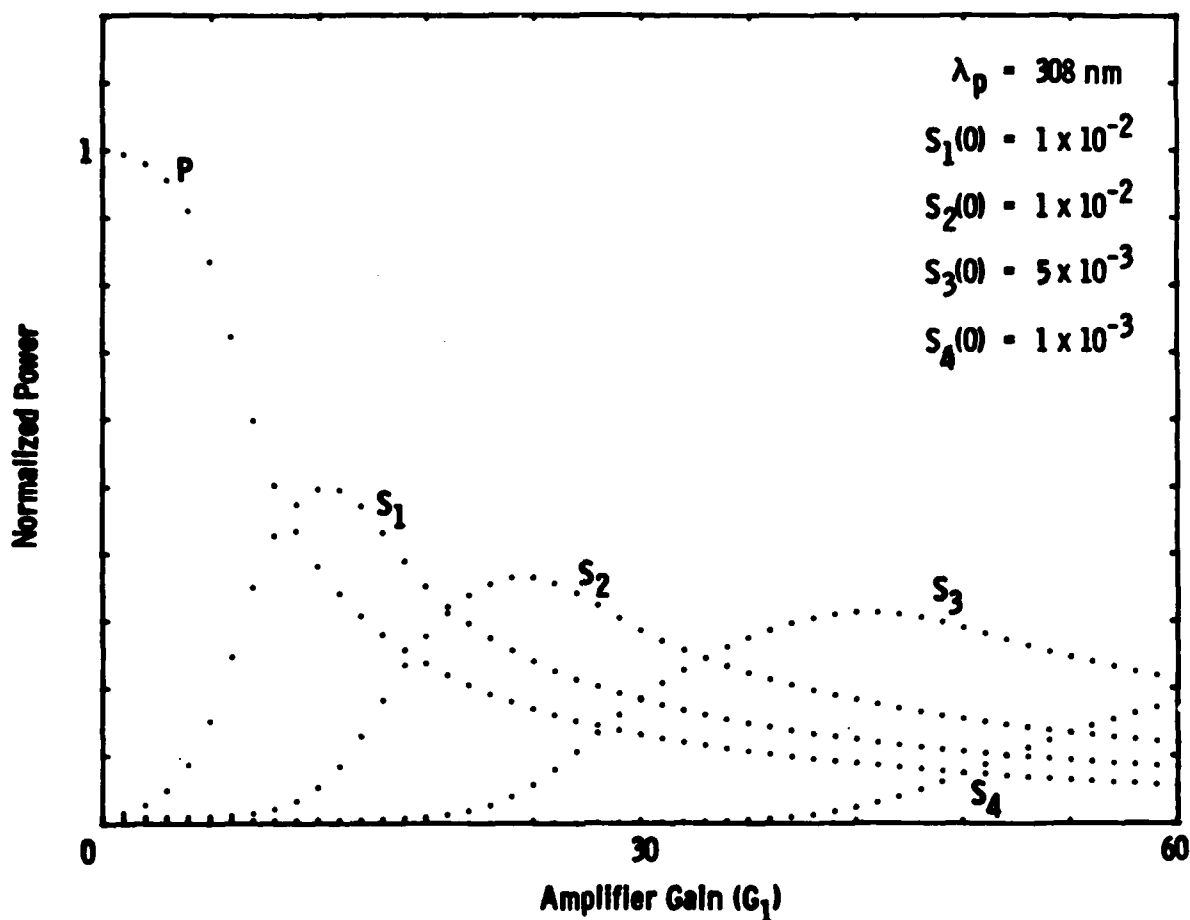


FIGURE 23. H₂ RAMAN AMPLIFIER POWER CONVERSION VS GAIN FOR GAUSSIAN BEAM PROFILE

It should be remarked that in a Raman oscillator the focused pumping is actually desirable in order to simultaneously generate multiple Stokes orders with the aid of four-wave mixing processes. However, in a Raman amplifier, a particular Stokes order is desired while suppressing conversion into the other orders or processes.

In summary, the experiments on H₂ Raman oscillator-amplifier system using the XeCl laser have demonstrated the feasibility of the third-order Raman converter concept for blue-green wavelength generation. Although the short pulse lengths and focused pumping configuration were employed in the present case, a 14 percent energy conversion from 308 nm to 499 nm has been observed in the

amplifier. Improvements on the efficiency are expected with longer pulses and collimated uniform beam profiles.

3.4 Nonlinear Dispersion in Broadband Amplifiers

Raman amplifiers pumped by a laser spectrum whose bandwidth is comparable to or larger than the Raman linewidth belong to a class of broadband amplifiers. In contrast to the monochromatic case, the broadband Raman gain depends on the frequency detuning from the line center. Furthermore, the real part of the nonlinear susceptibility tensor $\chi^{(3)}$ contributes to intensity dependent refractive index. For hydrogen, the measured $\chi^{(3)}$ for the $Q_{01}(1)$ transition is plotted in Figure 24. In this plot the imaginary part of $\chi^{(3)}$ is the Raman gain profile. The interaction of pump and Stokes radiation spectra via the real and imaginary parts of $\chi^{(3)}$ constitutes the basis of broadband amplifier analysis described below.

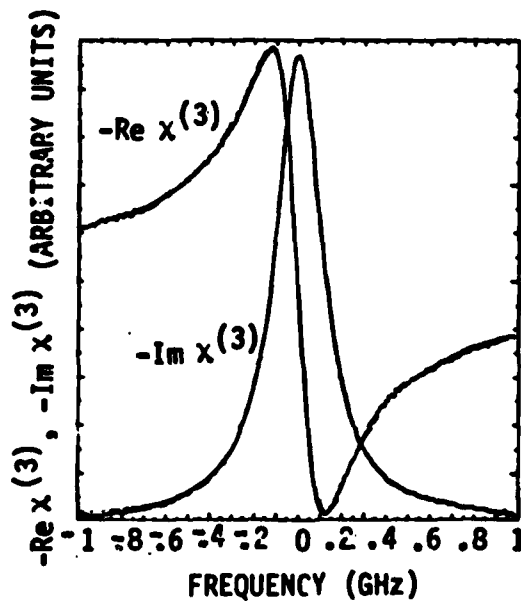


FIGURE 24. $\text{Re } \chi^{(3)}$ AND $\text{Im } \chi^{(3)}$ OF
 $\text{H}_2 Q_{01}(1)$ TRANSITION

(REF: A. OWYOUNG, -Opt. Lett. 3, 91, 1978)

3.4.1 Coupled-Mode Analysis

For the case of planewave interaction between broadband pump and Stokes radiation, the equations of electric fields are given by Eq. (1) - (3) in Section 3.2.1. According to these equations, the polarization at each Stokes and pump mode will, in general, have an inphase as well as a quadrature component, resulting in phase accumulation through the converter. The phase shift will be zero if in phase accumulation through the converter. The phase shift will be zero if

- Dispersion is absent
- Only the $n = 0$ term is important in the summation over n (i.e., $\gamma \gg \Gamma$ or δ -correlated waveforms) in Equations (2) and (3)
- The injected Stokes spectrum is proportional to the pump spectrum (temporal matching)

With these assumptions, the Stokes equation can be written as:

$$\frac{dv_j}{dx} = \frac{G_s}{2} u_j \sum_k v_k u_k^* \quad (11a)$$

Substituting $v_k = u_k^*(v/u)$ and $u_j = v_j^*(u/v)$ yields:

$$\frac{dv_j}{dx} = \frac{G_s}{2} v_j \sum_k |u_k|^2 \quad (11b)$$

showing that no phase is collected.

When the above conditions are not satisfied, usually because the second one is violated, the Stokes and pump waves will accumulate phase as they travel through the converter. The r.m.s. value of

this phase shift in the small signal regime is plotted versus the ratio of laser to Raman linewidth in Figure 25. Notice that the shift is largest for a small number of modes, but asymptotically disappears as $\Delta\omega_L/\Gamma \rightarrow \infty$, corresponding to δ -correlated spectra.

These nonlinear phase shifts represent a case of coupling between the temporal and spatial domains. Because they are intensity dependent, they lead to wavefront errors if the pump intensity profile is nonuniform. In Raman oscillators, which build up from noise, shifts of several radians can be accumulated in the small-signal regime. These shifts lead to beam focusing or defocusing, depending on the sign of the shift. As an example, in the case

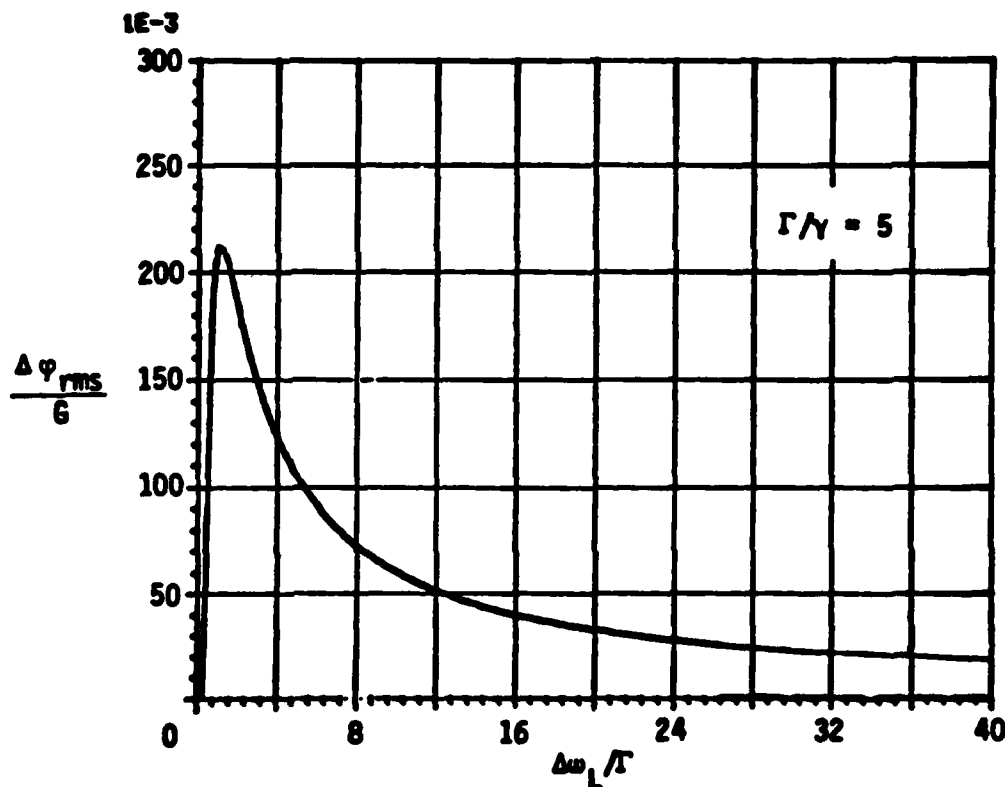


FIGURE 25 RMS INTENSITY-AVERAGED PHASE INCREMENT IN SMALL-SIGNAL REGIME

of defocusing, the beam area at the cell exit can be shown to increase by a factor of 2 when $\delta \sim b/(2L)$ where b is the confocal parameter of the pump beam and L the cell length. For a typical value of $b/L \sim 0.1$, this yields $\delta \sim 0.05$. Since this value is

much smaller than the actual shifts encountered, strong (de-focusing) effects are present in oscillators.

In Raman amplifiers, the saturated value of the phase shifts is important. Figure 26 shows the r.m.s. value of the accumulated Stokes phase obtained with a computer simulation of Equations (2) and (3). The number of laser modes was 51 and the number of modes under the Raman linewidth 5 in this simulation. The r.m.s. value corresponds to an average over modes for the given example. Notice how the phase increases to some maximum value and then decreases in the saturated regime.

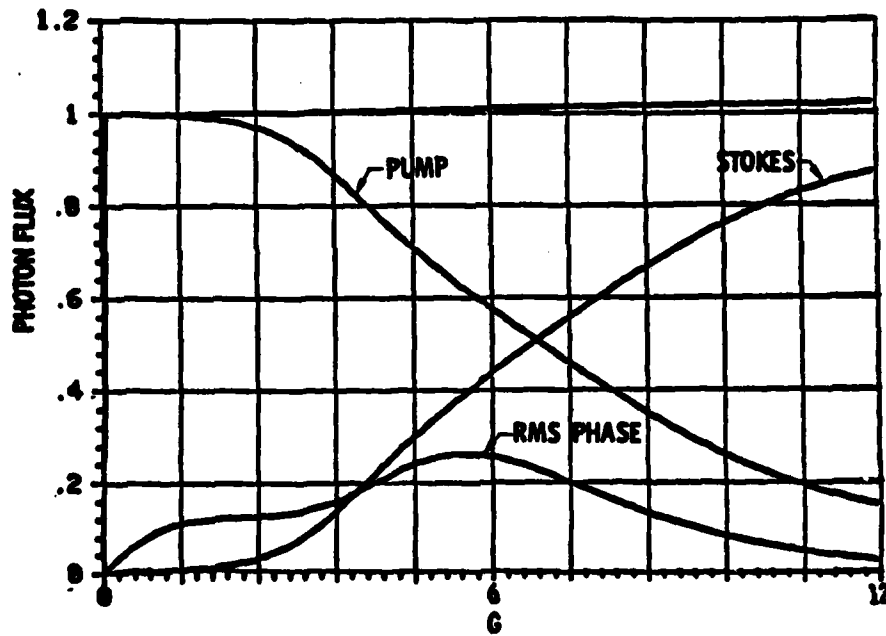


FIGURE 26 RMS PHASE IN SATURATED REGIME

3.4.2 Broadband Multiple Stokes Amplification

The coupled-mode equations developed and analyzed in the previous sections can be extended to model interaction of higher order Stokes shifted waves. All the physical processes of the first Stokes amplification are repeated in each successive Stokes shifts. In section 3.2.3, multiple-Stokes amplification of monochromatic pump and Stokes waves was discussed. It was also pointed out that broadband pumping can lead to Raman gains equal to the monochromatic case. This is found to be a limiting approximation for a large number of modes. This can be explained on the basis of the averaging effects in Equations (2) and (3) as mode number is increased. However, if the number of modes is not sufficient to smooth out the residual terms in the summations in Equations (2) and (3), the gain can be larger than the monochromatic case. Figure 27 illustrates this behavior. It is significant to note that even though the broadband Stokes amplification starts earlier than the monochromatic case the conversion efficiency does not reach the maximum value.

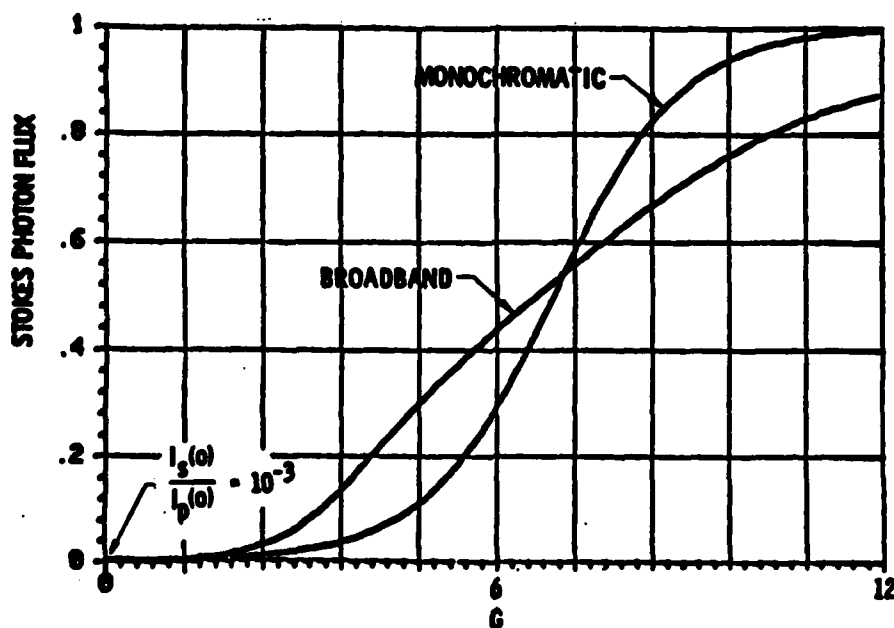


FIGURE 27 STOKES AMPLIFICATION DEPENDENCE ON PUMP SPECTRUM BANDWIDTH

The effect of this behavior on multiple Stokes amplification is illustrated in Figures 28 and 29 for two different laser bandwidths of 0.33 cm^{-1} and 0.67 cm^{-1} . The H_2 Raman linewidth was assumed to be $\Gamma = 0.012 \text{ cm}^{-1}$ at 6 amagats, and a typical laser mode spacing of $\gamma = 0.0033 \text{ cm}^{-1}$ was used. The Stokes injection intensities relative to the input pump intensity were chosen to be 4×10^{-3} , 4×10^{-3} , and 2×10^{-3} for the first, second, and third Stokes, respectively. All other Stokes orders were assumed to be zero.

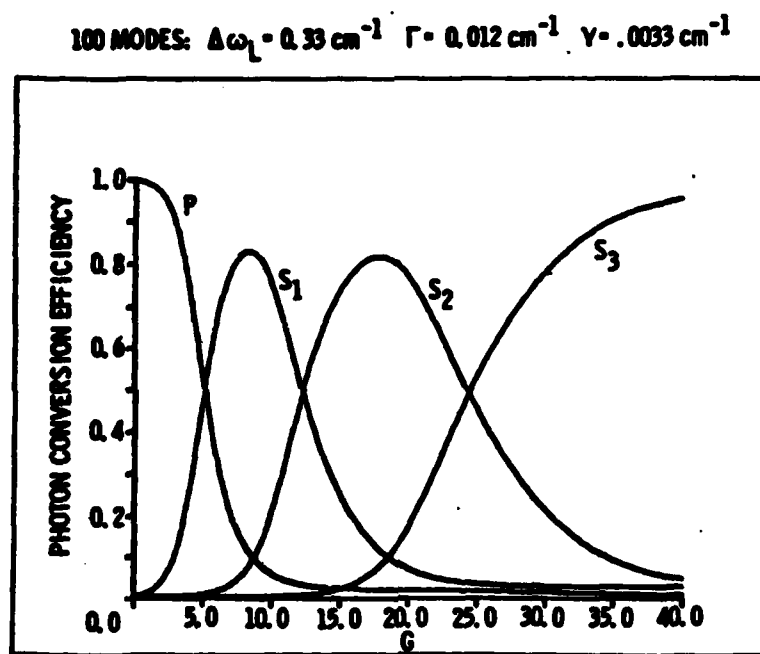


FIGURE 28 XeCl THIRD-STOKES CONVERSION IN HYDROGEN

In Figure 28 the number of laser modes is 100. The sequential amplification and conversion is similar to the monochromatic case of Figure 13, but the peaks of the S_1 and S_2 conversion are not quite optimized. The reduced conversion efficiency is due to the residual unconverted radiation in each successive Raman shift. This leads to a lower S_3 conversion efficiency. If the number of modes is increased to 200, Figure 29 indicates that residual unconverted radiation is significantly minimized. Consequently the S_3 efficiency approaches that of the monochromatic case.

These simulations indicate some subtle effects of polychromatic pumping which can lead to conversion efficiencies different from the approximations discussed in section 3.2.3.

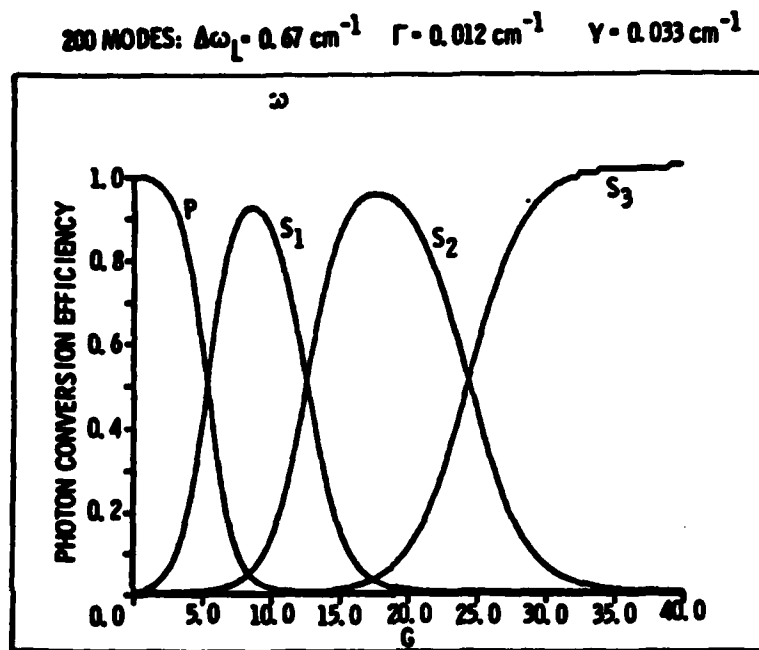


FIGURE 29 XeCl THIRD STOKES CONVERSION HYDROGEN

4.0 BLUE-GREEN RAMAN CONVERTER DESIGN

The experimental results and theoretical analyses of Raman conversion described in the previous section indicated that efficient UV-to-visible converters based on higher Stokes order shifting are feasible. These converters are a class of potentially viable blue-green lasers for underwater optical communication and other applications. For this reason a point design of a joule-level blue-green converter was generated.

The pump laser, in principle, can be any one of the efficient UV excimer lasers such as KrF, XeCl, and XeF. At the present time high efficiency and long lifetime of XeCl lasers make it an attractive pump laser. The required parameters for a representative XeCl laser as a joule-level Raman converter pump source are listed in Figure 30.

PARAMETER	VALUE	UNITS
WAVELENGTH	308.0	nm
BANDWIDTH	0.1	Å
PULSE LENGTH	60	ns
PULSE ENERGY	3.1	J
BEAM QUALITY	-3	x D. L.
BEAM DIVERGENCE	-0.03	mrad.
POLARIZATION	>95%	LINEAR
BEAM SHAPE: SQUARE / M - 3 CENTRAL OBSCURATION		

FIGURE 30 XeCl PUMP LASER CHARACTERISTICS
FOR A JOULE-LEVEL BLUE-GREEN CONVERTER

A Raman converter for the XeCl pump laser uses the third Stokes shift in H₂ which yields an output wavelength of 500 nm. In order to optimize conversion efficiency of an oscillator-amplifier scheme, the Stokes injection intensities must dominate over effective noise generated by four-wave mixing. This requirement may be satisfied by choosing the normalized injection levels

according to:

$$\eta_k \approx \left[\frac{g_k F l_k}{2\pi\tau} \right]^2 \quad (12)$$

where g_k is the k -th Stokes order gain coefficient, l_k is the coherence length of the k -th Stokes four-wave mixing, and F and τ are the pump beam fluence and pulse length, respectively. Using the known values of H_2 refractive indices [Ka64] and gain coefficient [Bi82], the normalized injection levels are on the order of 10^{-3} for a design pressure of 6 atmospheres and a fluence value of 1 J/cm^2 .

amplifier gain must be chosen appropriately. Figure 31 shows power conversion efficiency for the third Stokes output as a

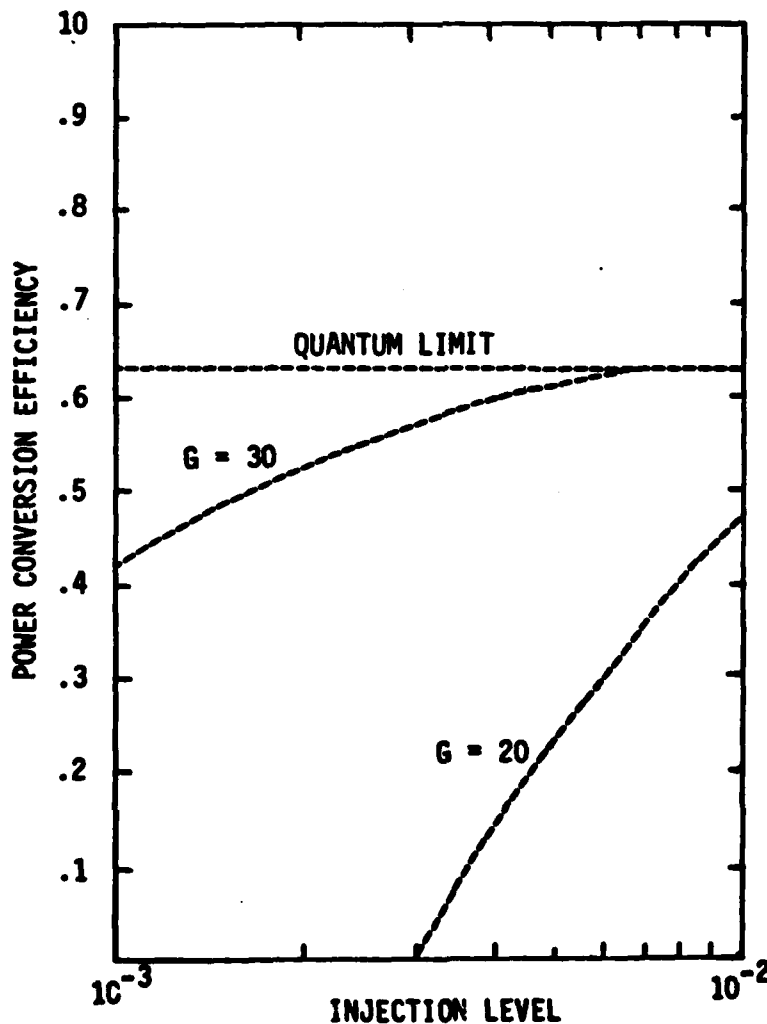


FIGURE 31 THIRD STOKES POWER CONVERSION EFFICIENCY VS. NORMALIZED INJECTION LEVEL

function of normalized injection levels, assuming that they are equal for the first three Stokes orders. It is clear that gains near $G=30$ are necessary for high efficiency operation. A flat-topped laser pulse is desirable to sustain a high efficiency value. However, in practice, the temporal variation of the laser pulse intensity directly changes the gain, and the energy conversion efficiency can be a sensitive function of the pulse shape. Figures 32 and 33 illustrate this dependence for a representative laser pulse shape and injection levels. Note that for a peak gain of $G=29$, the dominant conversion is still S_2 even though a significant amount of depletion is present at the middle of the pulse.

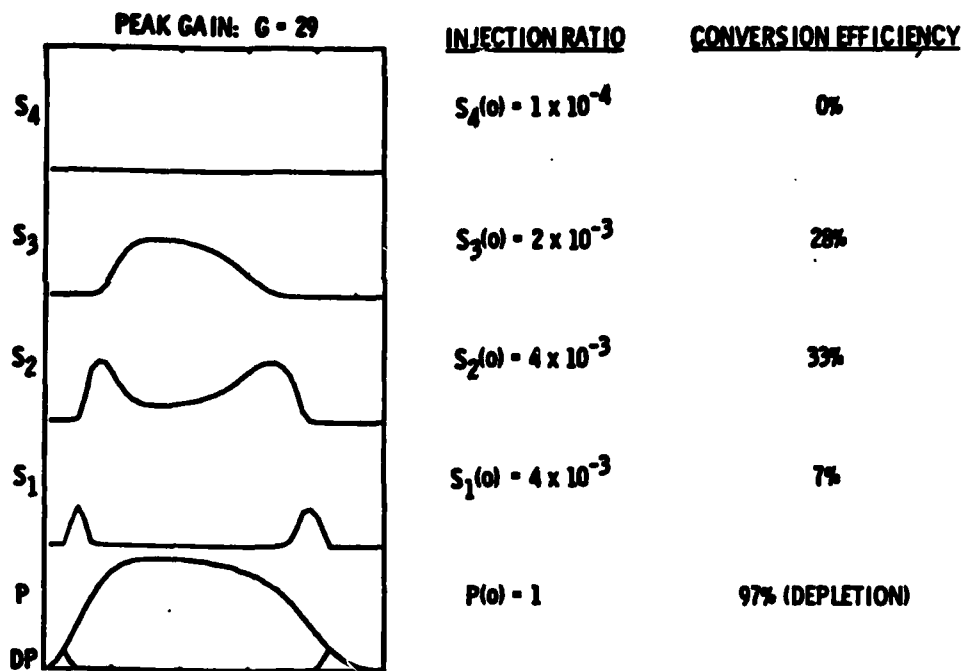
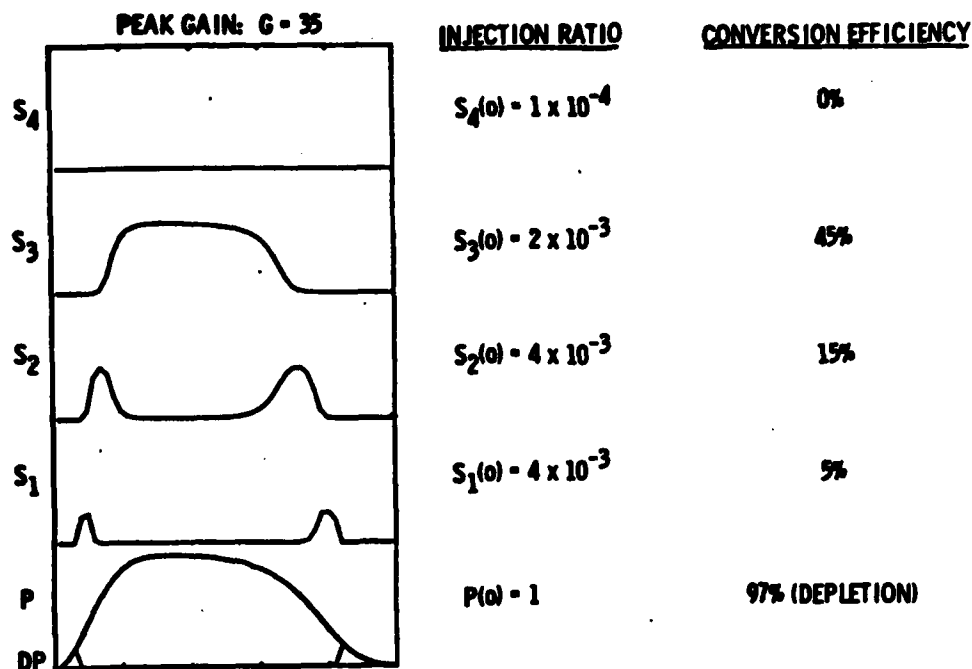


FIGURE 32 PULSE SHAPE AND ENERGY EFFICIENCY SIMULATION
FOR A PEAK GAIN OF $G = 29$

The reduced gains at the leading and trailing slopes of the pump pulse are responsible for this behavior. A small increase of the peak gain to $G=35$ in Figure 33 leads to a stronger S_2 depletion, and the S_3 energy conversion dominates over other Stokes orders. Therefore, it is critical to choose a proper peak gain value of a given laser pulse shape in order to optimize energy conversion efficiency.



**FIGURE 33 PULSE SHAPE AND ENERGY EFFICIENCY SIMULATION
FOR A PEAK GAIN OF $G = 35$**

Based on the above considerations, parameters of a point design are derived and listed in Figure 34.

PARAMETER	OSCILLATOR	AMPLIFIER	UNITS
CELL LENGTH	100	300	cm
H ₂ PRESSURE	6	6	atm
PUMP ENERGY	0.06 - 0.1	3	J
GAIN (S_1)	100	~ 30	---
FLUENCE	1	1	J / cm ²
BEAM AREA (WINDOW)	< 0.1	3	cm ²
PUMP BEAM FRESNEL NUMBER	< 3	333	---
PUMP / STOKES BEAM DIVERGENCE / OVERLAP	---	< 1	mrad.
STOKES OUTPUT S_1	.012	---	J
S_2	.012	---	J
S_3	.006	-1	J
PEAK POWER CONVERSION (S_3)	---	-60	%

**FIGURE 34 BLUE-GREEN RAMAN CONVERTER
POINT DESIGN PARAMETERS**

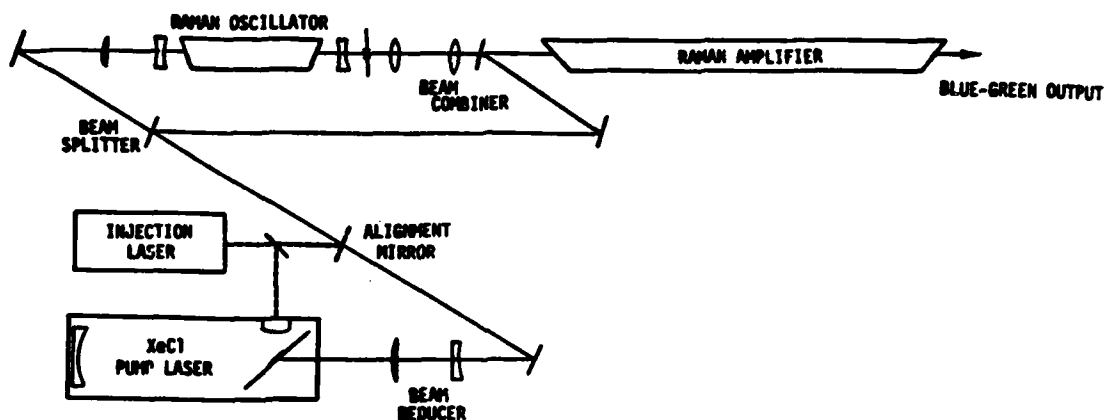


FIGURE 35 BLUE-GREEN RAMAN CONVERTER
POINT DESIGN SCHEMATIC

Figure 35 shows an optical schematic for this converter. The beam combiner is a long-wavelength-pass UV high reflector ($R > 99\%$) which can transmit 80% or more of the injected Stokes radiation. Each of the optical components are assumed to have figures of $\lambda/5$ for the UV (308 nm) and $\lambda/8$ for the blue-green (500 nm) wavelengths. These optical figure budgets translate to accumulated phase errors as listed in Figure 36. For single-pulse operation these phase errors lead to a Stokes beam quality near 6 times diffraction limit. If necessary a spatially filtered Stokes injection beam and better optics should enable near diffraction-limit beam quality.

COMPONENT	$\sum \Phi_{RMS}^2$ (RADIAN)
LASER	2.25
BEAM REDUCER / STEERING MIRROR	0.6
OSCILLATOR PUMP BEAM OPTICS	-4
STOKES INJECTION BEAM OPTICS	-3
AMPLIFIER PUMP BEAM OPTICS	-2.5

FIGURE 36 BLUE-GREEN RAMAN CONVERTER
POINT DESIGN OPTICAL TRAIN PHASE ERROR BUDGET

Under repetitively pulsed operation, thermal distortion of the optics must be considered. Furthermore, laser energy deposition in the H₂ cell by the stimulated Raman scattering process can cause thermal lensing effects, which will lead to suboptimal converter performance. Hence, a flowing gas cell is desirable for moderate to high average power operation.

5.0 CONCLUSIONS

The concept of higher Stokes order Raman shifting in H_2 based on an oscillator-amplifier scheme has been demonstrated to be an efficient means of generating visible (blue-green) output from a UV pump laser. Experimental investigations resulted in power conversion efficiencies near 30% into the third Stokes for the first time using a XeCl pump laser. Theoretical analyses on the effects of laser frequency bandwidth on Raman amplifier performance have led to the discovery and understanding of temporal (or spectral) correlation effects. Detailed computer code simulations based on these analyses made it possible to study nonlinear dispersion and multiple Stokes amplification under broadband pumping conditions. A key result of these calculations is that Raman conversion with broadband pump lasers is similar to the monochromatic case in the limit of large number of laser frequency modes. Hence efficient converters are feasible without having to narrow the pump laser spectrum to a single-mode output. A point design for a joule-level converter indicated that state-of-the-art technologies exist to build an efficient Raman shifted blue-green laser. Future work on flowing gas Raman cell technology should enable design of high average power visible lasers based on UV excimer down conversion.

6.0 REFERENCES

- [KS79] H. Komine and E. A. Stappaerts, "Efficient Higher Stokes Order Raman Conversion in Molecular Gases", Opt. Lett. 4, 398-400 (1979)
- [SLK80] E. A. Stappaerts, W. H. Long, Jr. and H. Komine, "Gain Enhancement in Raman Amplifiers with Broad-Band Pumping", Opt. Lett. 5, 4-6 (1980)
- [TPB79] W. R. Trutna, Jr., Y. K. Park, and R. L. Byer, "The Dependence of Raman Gain On Pump Bandwidth", IEEE J. Quant. Electron., QE-15, 648-655 (1979)
- [KS82] H. Komine and E. A. Stappaerts, "Higher-Stokes-Order Raman Conversion of XeCl Laser in Hydrogen", Opt. Lett. 7, 157-158 (1982)
- [BD78] R. Burnham and H. Djeu, "Efficient Raman Conversion of XeCl-laser Radiation in Metal Vapors", Opt. Lett. 3, 215-217 (1978)
- [LSB79] T. R. Loree, R. C. Sze, D. L. Barker, and P. B. Scott, "New Lines in the UV: SRS of Excimer laser Wavelengths", IEEE J. Quant. Electron., QE-15, 337-342 (1979)
- [GZ78] A. Z. Grasiuk and I. G. Zubarev, "High-Power Tunable IR Raman Lasers", Appl. Phys. 17, 211-232 (1978)
- [Ka64] M. Karplus, "Refractive Index of the Hydrogen Molecule", J. Chem. Phys. 41, 880-883 (1964)
- [Bi82] W. Bischel, private communication

END